

Numerical Study of Debris Flight in a Tornado-like Vortex

Huo, Ryan; Hemida, Hassan; Sterling, Mark

License:

Creative Commons: Attribution-NonCommercial-NoDerivs (CC BY-NC-ND)

Document Version

Peer reviewed version

Citation for published version (Harvard):

Huo, R, Hemida, H & Sterling, M 2020, 'Numerical Study of Debris Flight in a Tornado-like Vortex', *Journal of Fluids and Structures*.

[Link to publication on Research at Birmingham portal](#)

General rights

Unless a licence is specified above, all rights (including copyright and moral rights) in this document are retained by the authors and/or the copyright holders. The express permission of the copyright holder must be obtained for any use of this material other than for purposes permitted by law.

- Users may freely distribute the URL that is used to identify this publication.
- Users may download and/or print one copy of the publication from the University of Birmingham research portal for the purpose of private study or non-commercial research.
- User may use extracts from the document in line with the concept of 'fair dealing' under the Copyright, Designs and Patents Act 1988 (?)
- Users may not further distribute the material nor use it for the purposes of commercial gain.

Where a licence is displayed above, please note the terms and conditions of the licence govern your use of this document.

When citing, please reference the published version.

Take down policy

While the University of Birmingham exercises care and attention in making items available there are rare occasions when an item has been uploaded in error or has been deemed to be commercially or otherwise sensitive.

If you believe that this is the case for this document, please contact UBIRA@lists.bham.ac.uk providing details and we will remove access to the work immediately and investigate.

Manuscript Details

Manuscript number YJFLS_2020_84_R1
Title Numerical Study of Debris Flight in a Tornado-like Vortex
Article type Research Paper

Abstract

This paper presents the numerical study on the flight behaviour of spherical compact debris in a tornado-like wind field. The tornado-like vortex corresponding to a swirl ratio of 0.7 was generated using Large-eddy Simulation and the trajectories of 2250 individual debris particles placed in the flow were computed using Lagrangian-particle tracking. The debris corresponded to five groups (A, B1, B2, B3 and C) based on the value of the Tachikawa number (K) which ranged between 0.6 and 2.5. An analysis of the simulated flow field revealed that the tornado-like vortex consisted of two main features - a core at the centre with low velocity ($\sim 0.25\text{m/s}$) which was surrounded by thick vortex wall composed of high velocity magnitudes ($\sim 9.4\text{m/s}$). Updraft flows were observed around the core of the vortex and as a result, debris positioned around the core radius region were found to be 24% more likely to become wind-borne than debris positioned at the vortex wall region. Three groups of debris (B1, B2 and B3) with varying mass and density were studied for the aerodynamic similarity by retaining the fixed value of $K=1.2$; all three debris groups exhibited the propensity to travel with similar flight characteristics. An analysis of the data pertaining to the flight behaviour of the three debris group (A, B1 and C) with varying K revealed that the low mass debris group A ($K=2.5$) had the highest propensity to become wind-borne and was more likely to travel for the longest time with considerable variability observed in individual debris trajectories. However, somewhat counterintuitively, the high mass debris group C ($K=0.6$) were found to have the furthest impact range despite their short flight duration; this was due the high mass debris being ejected out of the vortex with greater inertia, while debris with a lower mass had a tendency to be trapped in the flow that circulates around the vortex core.

Keywords CFD; flying Debris; tornado-like vortex; large eddy simulation

Corresponding Author Shuan Huo

Corresponding Author's Institution University of Birmingham

Order of Authors Shuan Huo, Hassan Hemida, Mark Sterling

Submission Files Included in this PDF

File Name [File Type]

Cover letter.doc [Cover Letter]

Responses to reviewers comments.docx [Response to Reviewers]

Numerical Study of Debris in Tornado-like Vortex (clean).docx [Manuscript File]

declaration-of-competing-interests.docx [Conflict of Interest]

CRedit author statement.docx [Author Statement]

Numerical Study of Debris in Tornado-like Vortex (tracked changes).docx [Supplementary Material]

Submission Files Not Included in this PDF

File Name [File Type]

Figure 1.png [Figure]

Figure 2.png [Figure]

Figure 3.png [Figure]

Figure 4.png [Figure]

Figure 5.png [Figure]

Figure 6.png [Figure]

Figure 7.png [Figure]

Figure 8.png [Figure]

Figure 9.png [Figure]

Figure 10.png [Figure]

Figure 11.png [Figure]

Figure 12.png [Figure]

Figure 13.png [Figure]

Figure 14.png [Figure]

Figure 15.png [Figure]

Figure 16.png [Figure]

To view all the submission files, including those not included in the PDF, click on the manuscript title on your EVISE Homepage, then click 'Download zip file'.

Research Data Related to this Submission

There are no linked research data sets for this submission. The following reason is given:
Data will be made available on request

1
2
3
4
5
6
7
8
9
10
11
12
13
14
15
16
17
18
19
20
21
22
23
24
25
26
27
28
29
30
31
32
33
34
35
36
37
38
39
40
41
42
43
44
45
46
47
48
49
50
51
52
53
54
55
56

Mr Shuan Huo
University of Birmingham
School of Engineering
University of Birmingham
Edgbaston
Birmingham
B15 2TT
UK

9th February 2020

Dear Professor Langre,

We wish to submit a full-length research article entitled “Numerical Study on Debris Flight in a Tornado-like Vortex” by Shuan Huo, Hassan Hemida and Mark Sterling for possible publication in the Journal of Fluids and Structures.

We confirm that this work is original and has not been published elsewhere, nor is it currently under consideration for publication elsewhere.

Please address all correspondence concerning this manuscript to me at srh629@bham.ac.uk.

Thank you for your consideration of this manuscript. I look forward to hearing from you in due course when the review process has been completed.

Yours sincerely,

Shuan Huo
Ph.D Student
Department of Civil Engineering
School of Engineering
University of Birmingham

1
2
3
4 The authors would like to thank the reviewers for their comments which have given us an opportunity
5 to reflect on the paper and make adjustments. In what follows we address and embrace the comments
6 by both reviewers. Two versions of the paper are provided – a clean version and a tracked changes
7 version indicating where the text has been altered. For the benefit of the reviewers, changes are listed
8 below with new text highlighted using a yellow background.

9
10
11 **Reviewer 1**

12
13
14 This paper presents a numerical study of debris flight in a tornado-like flow. The conditions for the
15 initialization of the flight and the impacts of the flow and debris characteristics on the flight trajectory
16 are comprehensively investigated. Part of the numerical results are compared to previously published
17 experimental results. Since there have only been few studies of debris flights in tornadoes, the
18 outcomes presented in this paper can be valuable for subsequent studies. However, the reviewer does
19 recommend that two major problems and a number of minor problems be addressed before the paper
20 can be published in Journal of Fluids and Structures.

21
22 Major problems:

23
24 1. The reviewer believe that the paper should be more willing to acknowledge the limitations of the
25 numerical study instead of liberally brushing these limitations and in many places simply saying the
26 numerical results are good even when such an assessment is not warranted.

27
28 Examples include but are not limited to:

29
30 (1) The paper suggests that the numerical and experimental results presented in Figure 6 agree
31 very well and that there are only minor differences around the core region. However, a simple
32 inspection of this figure can reveal quite significant differences between the numerical and
33 experimental profiles, even in regions away from the core. Moreover, the paper simply
34 attributes the differences to the uncertainty of the experiments. This, to the reviewer, is a little
35 cavalier, as computational fluid dynamics based simulations are to date far from perfect.

36
37 The fully authors agree and acknowledge that in places they make have not been as reflective
38 as they should have been, for that we apologise.

39
40 New text has been added to **line 193 - 196** as follows:

41
42 ...figure 2. Whilst every effort has been made to accurately reproduce the physical simulator
43 their will inevitably be small differences introduced due to the meshing process. It is
44 difficult to quantify the impact of these differences, but in what follows it is assumed that
45 beyond a certain mesh resolution their effects are negligible (see section 3).

46
47 The following change has been made to **lines 291 - 300**

48
49 Overall, the predicted velocity field matches that given by the physical results. However,
50 both the numerical and physical simulations are not without their limitations: accurately
51 specifying inflow boundary conditions are crucial for LES yet fraught potentially with
52 difficulties (Yang, 2015), as very specific information on turbulence is required to reproduce
53 identical inflows, e.g., turbulence intensity, stochastically varying turbulent length scales,
54 and power spectrums of turbulent etc. The effects of SGS modelling is also considered to be
55 a potential source of uncertainty since SGS motions inevitably requires unrealistically fine
56
57
58
59

60
61
62 cells at all regions even locations far away from the vortex structure. Notwithstanding these
63 limitations, the numerical results presented in the paper are within the range of experimental
64 uncertainty and considered suitable for the purposes of this work

65
66 **Page 14, line 360 - 361** now read:

67
68 Both the numerical and experimental results correspond well (considering the uncertainty
69 associated with the results) at the location $r/r_c=1$ with the overlapping trajectory path of
70 approximately 78%; while at the location $r/r_c=2$, the overlapping region was lower at
71 approximately 61%

72
73 And **page 20, line 500** now read:

74
75 Acknowledging the uncertainty associated with the data, the numerical simulations agree
76 well with previous experimental research and provide a greater insight into the flow field.

77
78
79 (2) In the discussion regarding Figure 9, apparent differences again exist between the numerical
80 and experimental results. However, the paper states that the numerical and experimental results
81 “correspond well” and again attributes the differences only to the “the larger variation in the
82 trajectory paths from the experiments, caused by the turbulent fluctuation in the local field.”
83 Shouldn’t the numerical simulation faithfully reproduce the turbulent fluctuation in the local
84 field? How well does the numerically simulated turbulence compare with the turbulence
85 measured in the experiments?
86
87

88 The authors agree (in part), but note that given the uncertainties now acknowledged a faithful
89 reproduction of the physical data in all of the domain is unlikely. In addition, we note that
90 turbulent intensities were not compared to the experiments due to the absence of the latter in
91 the papers (associated with the difficulties of obtaining reliable measurements) (Gillmeier et
92 al., 2017; Bourriez et al., 2017). Thus, we have adjusted the text as follows (**page 15, line**
93 **386 - 395**):

94
95
96
97 In general, the prediction of debris trajectories corresponds well for both the numerical
98 simulation and experiments results; however, it should be pointed out that debris were
99 assumed to be one-way coupled and the motion of debris were also assumed with no rotation
100 in a highly swirling flow, which may result in some difference in overall trajectories between
101 numerical and physical simulation. We also note the lack of turbulence data associated with
102 the physical measurements results in an uncertainty of the flow simulation in this region.
103 Notwithstanding this the numerical simulation are consistent with the physical data and able
104 to capture the entire flight duration from initialization to the impact on the ground.
105 Furthermore, the numerical simulations provide a better understanding of the impact
106 distribution and extend the results of the physical simulation.
107
108

109
110
111 2. The paper suggests flight initializations occur mainly in regions where updrafts are present. Can
112 this be due to the oversimplification of the problem? First, the study assumes that the debris does not
113 rotate. This can be very different from reality, especially in the presence of a flow field that is very
114 three dimensional and inhomogeneous, and lead to oversimplification of the interaction between the
115 fluid and the debris. Also, how well does the numerical model simulate the interaction between the
116
117
118

119
120
121 debris and the flow even with the assumption? The reviewer understands the challenges involved and
122 is not suggesting that the paper should not be published given the limitations. However, the paper
123 should at least acknowledge these limitations.
124

125 The authors appreciate this question and it is something that they have long pondered. Inspection
126 of the debris corresponding to the physical data suggests that this may not be the case due to the
127 relative size of the debris and the curvature of the streamlines – we acknowledge that the
128 resolution of the physical data is limited in this regard (and probably would not stand up to
129 rigorous peer review) so we cannot be certain, but this is our current working assumption. We also
130 note that this is a working assumption which has been embraced by others (Holmes, 2004; Baker,
131 2007; Wills et al., 2002) who have concluded that the trajectories and velocities can be reasonably
132 predicted by only considering the action of the drag force and gravitational force acting on the
133 debris. However, we also acknowledge that this area of research is very much in its infancy. On
134 reflection, we agree that this should be acknowledged in the paper and as such have introduced
135 new text as follows (page 20, line 529 - 534):
136
137

138 It is worth noting that current study only considers the flow field of the vortex at $S=0.7$. Different
139 swirl ratios have the potential to result in different flow characteristics and those would affect the
140 overall behaviour of wind-borne trajectory. Further, the flight characteristics of debris were
141 assumed with no rotation, which might be considered less realistic in a highly swirling vortex flow
142 field when the rotation of debris generates lift, which would lead to a different interaction between
143 the fluid and debris.
144

145
146
147 We have also highlighted the lack of rotation of the particles in a number of other locations in the
148 text, but have not listed these below (e.g., see line 202, line 389, and line 532).
149

150
151
152 Less significant problems:

- 153
154 1. The paper provides two inconsistent definitions of the aspect ratio: one from line 115 to line 116,
155 and the other according to equation (2).

156 This was an oversight on our part which has now been corrected. (page 4, line 130 - 133):
157

$$158 \quad S = \frac{\tan\theta}{2a} \quad [1]$$

159
160 where θ is the guide vanes angles and a is the aspect ratio, defined as:
161

$$162 \quad a = \frac{2h_2}{D_3} \quad [2]$$

163
164 The definition of the aspect ratio is based on the physical dimensions of the simulator; the ratio
165 between the diameter of the exhaust outlet (D_3) and the height of the inlet (h_2).
166

- 167
168
169
170
171 2. Lines 156-157: The descriptions of the axes are not correct.

172 The descriptions of the axes have been adjusted (page 5, line 161 to 163):
173
174
175
176
177

178
179
180 where the xy plane represents the horizontal plane while z axis represents the axis perpendicular to
181 the horizontal plane.
182
183
184

185 3. What are the shapes of the debris? Are those spheres since only the diameters are given?
186

187 The reviewer is correct; the geometric configurations of the debris are spheres. Additional
188 descriptions have been added. (line 13 and line 201):
189

190 This paper presents the numerical study on the flight behaviour of spherical compact debris in a
191 tornado-like wind field.
192

193 And
194

195 Each individual debris was assumed to be a three dimensional spherical compact
196
197
198
199
200
201
202
203
204
205
206
207
208
209
210
211
212
213
214
215
216
217
218
219
220
221
222
223
224
225
226
227
228
229
230
231
232
233
234
235
236

237
238
239 **Reviewer 2**
240
241
242

243 The rationale behind the LES simulation for tornadic like vortex flow simulation was well explained,
244 carried out with OpenFOAM. The CFD simulation domain was modelled after the Birmingham
245 simulator, with experimental results from Gillmeier used as validation. Mesh convergence study was
246 carried out to determine the flow structure sensitivity.
247

248 Airborne debris simulations were based on experimental tests performed at the University of
249 Birmingham and showed good agreement. Conclusions drawn on the flight time as a function of
250 Tachikawa number (K) and debris impact location were unique and useful contributions to the field of
251 tornado research. The conclusions made are sensible based on the fluid mechanics of the tornado
252 vortex.
253

254 Overall the paper is worthy of publication, but there are minor comments that should be addressed
255 before the paper is published. In summary:
256

257 1. No explanation was given as to why a swirl ratio of 0.7 was selected for the study. I'm assuming
258 that it was due to limited experimental data made available to them, but I would think that this
259 parameter would have very important implications on the resulting trajectory and flight times or the
260 airborne debris.
261

262 The reviewer is correct on the selection of the swirl ratio and their assumption. We have
263 undertaken both physical and numerical simulations for another swirl ratio but chose not to include
264 the results in order to keep the paper a reasonable length. We adjusted the text as follows to
265 acknowledge the reviewer's point (page 20, line 529 - 531):
266

267 It is worth noting that current study only considers the flow field of the vortex at $S=0.7$. Different
268 swirl ratios have the potential to result in different flow characteristics and those would affect the
269 overall behaviour of wind-borne trajectory.
270
271
272

273 2. The aspect ratio definition based on the physical dimensions of the test apparatus which may lead
274 to a different aspect ratio if the tornadic fluid structure instead. Gairola and Bitsuamlak 2019 (JWEIA)
275 has modelled three different tornado testing chambers (UWO, IOWA, TEXAS TECH) and discussed
276 this aspect ratio issue, can you comment how the aspect ratio defined using the Birmingham testing
277 apparatus fits with others?
278

279 The authors are incredibly comforted by the fact that the reviewer has raised this point since it
280 proves that others are starting to appreciate this fact as well. For the last few years this is an issue
281 that we have also been raising at many international conferences, is what Gillmeier based her PhD
282 thesis on and is formally stated in a peer review journal (Gillmeier et al. 2019). It is thus with
283 great pleasure that we add the following text (page 20, lines 533 – 536 and page 4, line 133 -
284 136):
285

286 ... which would lead to a different interaction between the fluid and debris. It is also worth noting
287 that this work has simulated the flow assuming one single definition of aspect ratio, but as
288 indicated by Gillmeier et al. (2019) and Gairola and Bitsuamlak (2019), this may be an important
289 area which has hitherto largely been neglected.
290
291
292
293
294
295

296
297
298 By the way, this reviewer noticed notable tornado related papers missing in the reference including
299 the one mentioned here.
300

301 We have included a number of references and would happily include more if we have missed a
302 notable reference which is relevant to the current work. However, there has been a trend of late
303 (particularly in a certain journal) to include papers for the sake of name checking certain authors.
304 We are not averse to adding more references of direct relevance, but the reviewer would need to
305 tell us what notable papers we are missing.
306

307
308
309 3. Within the literature review, it was stated that Ward-type tornado simulators were unable to provide
310 reliable and accurate insights into the vortex flow structure. I believe that this is a misleading
311 comment, but rather the Ward simulators were limited by their size and design to reproduce some
312 characteristics of tornado flow (such as translating effects), but were effective in investigating other
313 characteristics.
314

315 The following text has now been added (page 2, lines 46 - 48):
316

317 ...vortex and provided an alternative to study tornado flows. However, Ward's simulators were
318 limited by their size unable to reproduce some vortex characteristics due to the design.
319

320
321
322 4. Abstract: tornado like "vortex" is missing
323

324 This was an oversight on our part which has now been corrected.
325
326

327 5. The low percentage of windborne debris were attributed to ignoring the translation effects of the
328 tornado, can you add a context how much velocity are we missing from the translation that affects the
329 result. (see line 306-309).
330

331 The context of translating speed have been provided in the revised manuscript as requested. (page
332 11, line 322 to 327)
333

334 The low percentage of windborne debris were not too surprising as this study focuses only on the
335 wind-borne behaviour in a stationary tornado, where the translation effects of the tornado were
336 ignored. However, it is worth nothing that the translational movement of a naturally occurring
337 tornado could potentially result in higher percentage of debris becoming wind-borne; several
338 researches (Kosiba et al., 2014; Matsui et al., 2008; Phuc et al., 2012) have been carried out where
339 the translating speed of tornado ranges from $0.05 U_T$ to $0.7 U_T$.
340
341
342
343
344
345
346
347
348
349
350
351
352
353
354

Numerical Study of Debris Flight in a Tornado-like Vortex

Shuan Huo^{*1)}, Hassan Hemida²⁾, Mark Sterling³⁾

*Department of Civil Engineering, School of Engineering, University of Birmingham, Birmingham,
United Kingdom*

*1) *srh629@bham.ac.uk*

2) *h.hemida@bham.ac.uk*

3) *m.sterling@bham.ac.uk*

Abstract

This paper presents the numerical study on the flight behaviour of spherical compact debris in a tornado-like wind field. The tornado-like vortex corresponding to a swirl ratio of 0.7 was generated using Large-eddy Simulation and the trajectories of 2250 individual debris particles placed in the flow were computed using Lagrangian-particle tracking. The debris corresponded to five groups (A, B1, B2, B3 and C) based on the value of the Tachikawa number (K) which ranged between 0.6 and 2.5. An analysis of the simulated flow field revealed that the tornado-like vortex consisted of two main features - a core at the centre with low velocity ($\sim 0.25\text{m/s}$) which was surrounded by thick vortex wall composed of high velocity magnitudes ($\sim 9.4\text{m/s}$). Updraft flows were observed around the core of the vortex and as a result, debris positioned around the core radius region were found to be 24% more likely to become wind-borne than debris positioned at the vortex wall region. Three groups of debris (B1, B2 and B3) with varying mass and density were studied for the aerodynamic similarity by retaining the fixed value of $K=1.2$; all three debris groups exhibited the propensity to travel with similar flight characteristics. An analysis of the data pertaining to the flight behaviour of the three debris group (A, B1 and C) with varying K revealed that the low mass debris group A ($K=2.5$) had the highest propensity to become wind-borne and was more likely to travel for the longest time with considerable variability observed in individual debris trajectories. However, somewhat counterintuitively, the high mass debris group C ($K=0.6$) were found to have the furthest impact range despite their short flight duration; this was due the high mass debris being ejected out of the vortex with greater inertia, while debris with a lower mass had a tendency to be trapped in the flow that circulates around the vortex core.

1. INTRODUCTION

Tornadoes are perhaps one of the most destructive weather phenomena due to their potentially violent and unpredictability nature. The wind speeds of a tornado can reach up to 450 kilometres per hour and can cause severe damage to civil structures and loss of lives. In March 2019, a tornado struck the Lee County in Alabama (USA) and caused catastrophic damage around the region: it was reported that the tornado was classed as an EF4 with wind speeds reaching 270 kilometres per hour (Darrow, 2019) and claimed the lives of more than 23 people. Tornadoes are complex phenomena and despite their frequent occurrence, surprisingly little is known about the flow structure. Due to the violent nature and unpredictable path of tornadoes, details of the tornado flow field using full scaled methods have, to date, proved to be rather elusive; therefore, recourse is often made through physical and numerical modelling. The earliest systematic experiment for generating laboratory-scaled tornado-like vortices can perhaps be attributed to Ward (1972). Ward developed a laboratory simulator with an exhaust fan at the top to provide updraft flow and vanes at the ground to generate angular momentum. This approach enabled the reproduction of tornado-like flow from a single-celled vortex

46 into a multi-celled vortex and provided an alternative to study tornado flows. However, Ward's
47 simulators were limited by their size unable to reproduce some vortex characteristics due to the
48 design. Therefore, an increasing number of studies have been conducted in order to numerically
49 simulate such flow.

50 Recent numerical studies have been conducted extensively to study the flow fields of tornado-like
51 vortices. Howells et al. (1988) and Nolan and Farrell (1999) used the axisymmetric Navier-Stokes
52 equations in cylindrical coordinates to examine the flow structure of a tornado-like vortex. Lewellen
53 et al. (1999) conducted Large-eddy Simulation (LES) to examine the interaction between the
54 generated vortex and the surface roughness. Unsteady Reynolds-Averaged Navier-Stokes (URANS)
55 model for the numerical simulation were performed by Hangan and Kim (2006) to reproduce tornado-
56 like vortices. They concluded that the core of the tornado was the most difficult region to properly
57 reproduce. Lewellen and Lewellen (2007) employed a LES turbulence model to study the effects of
58 swirl ratio (a parameter which measures the strength of a circulation relative to the updraft flow) on
59 vortex structure and translation speed. Kuai et al. (2008) conducted numerical research on full scale
60 and laboratory simulated tornadoes using the k- ϵ turbulence model and verified the ability of
61 numerical methods to capture the flow fields of the tornadoes. Hangan and Kim (2008) conducted
62 simulations using an URANS model to reproduce tornadoes at different swirl ratios, and discovered
63 that a high swirl ratio corresponded with full scale data from the Spencer tornado observed by
64 Alexander and Wurman (2005). Ishihara et al. (2011) compared the flow fields of two different types
65 of vortices and validated the results with the laboratory experiments. Natarajan (2011) numerically
66 simulated different stages of tornadoes and confirmed the findings from earlier physical simulations
67 is the primary governing parameter of a vortex. Research undertaken by Ishihara and Liu (2014)
68 conducted an in-depth study of a tornado-like vortex during touch down stage with detailed analysis
69 of the flow field; while Liu and Ishihara (2015) further investigated the stages of tornado-like vortices
70 in order to capture of characteristics of the evolution of different vortex stage. The excellent research
71 conducted by the aforementioned researchers and others provides an insight to tornado flows and its
72 mechanism; however, the definition of the swirl ratio from these studies varies from one to another,
73 therefore, detailed discussions on the definition of swirl ratio employed in this study were discussed
74 in section 2.2.

75 Another key factor that contributes to the tornado induced damage is flying debris. Everyday objects
76 can become damaging projectiles when subject to a tornado, and individuals have been affected
77 considerably by debris which become windborne as a result of a tornado (Harms, 2019). Numerous
78 research on flying debris have been undertaken since the pioneering works of Tachikawa (1983), which
79 proposed a dimensionless parameter, K , which describes the ratio between the inertial forces of the
80 flow to the weight of the debris. Wills et al. (2002) categorized debris based on their respective
81 damage performance with light, medium or heavy weight missiles; other identification based on the
82 geometrical structure can further categorize the debris into compact type (3D), plate type (2D) and
83 rod type (1D). Further work on the trajectories of compact type (3D) spherical debris in strong winds
84 was conducted by Holmes (2004) and English (2005). Baker (2007) also generalized the equations of
85 motion for debris flight in dimensionless form for compact and sheet-like debris. Furthermore, plate-
86 like (2D) debris (Tachikawa, 1983; Wang and Letchford, 2003; Holmes et al., 2004) and rod-like (1D)
87 debris (Lin et al., 2007; Richards et al., 2008) under different wind conditions have also been studied
88 extensively, but none of these studies were carried out under tornado-like flow conditions. Recently,
89 several investigations on debris flight in tornadoes have been conducted; Maruyama (2011) simulated
90 a tornado-like vortex using large eddy simulations with the statistical distribution of debris velocities.
91 Bourriez et al. (2017) studied the flight paths of debris in laboratory controlled conditions. Research
92 undertaken by Baker and Sterling (2017) provided an analytical model for the velocity and pressure

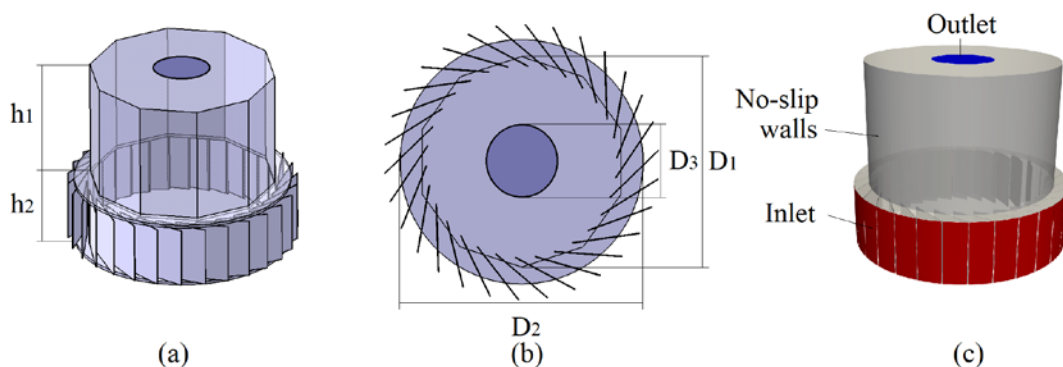
93 fields of tornadoes as well as the prediction of debris trajectories within the tornado. While these
94 studies provide a great insight to the flow fields and trajectories, there is a lack of detailed analysis on
95 flying debris in tornadoes. Hence, the objective of the present work was to investigate the behaviour
96 of flying debris in a tornado-like wind field. The tornado-like vortex was simulated using LES. The flow
97 fields of the vortex were analysed and the characteristics features were presented. Trajectories of five
98 debris groups with varying Tachikawa number were computed and the flight data were analysed.

99 The paper is organized as follows: Section 2 describes the procedure adopted and the numerical
100 details relating to this. Section 3 outlines the three dimensional flow field, characteristics and
101 mechanisms of the simulated tornado-like vortex. The detailed analysis of debris flight in tornado wind
102 field were discussed in section 4. Appropriate conclusions are given in section 5.

103 2. METHODOLOGY

104 2.1 DESCRIPTION OF PHYSICAL SIMULATOR

105 The model used in the current research was based on the University of Birmingham Tornado Vortex
106 Generator (UoB-TVG), shown in figure 1. A series of physical simulations were undertaken by Gillmeier
107 et al. (2017) and were used as validation for the numerical flow field simulated in the current paper.
108 The UoB-TVG was a large-scale Ward-type vortex generator based on the design of Ward's simulator
109 (Ward, 1972) with exhaust fans placed at the top of the convection chamber that were used to
110 generate an updraft flow. Situated below the convection chamber was the convergence chamber,
111 designed to draw air inwards with a series of guide vanes mounted at the edge of convergence
112 chamber. Angular momentum was obtained by setting the guide vanes to different angles, thus
113 generating different vortex structures. The convection chamber has the height, h_1 of 2m and diameter,
114 D_1 of 3.1m and convergence chamber with the height, h_2 of 1m and diameter, D_2 of 3.6m with thirty
115 guide vanes mounted around the edges of the convergence chamber. An exhaust outlet with
116 diameter, D_3 of 1m was situated at the top of the convection chamber. The ratio between updraft
117 diameter and the height of the convergence chamber was defined as the aspect ratio, a . The velocity
118 at the inlet (U_∞) was 0.66m/s, which was computed based on the measured total outflow rate (Q) of
119 $7.38 \text{ m}^3/\text{s}$ at the exhaust outlet. The velocity measurements of the flow field were made 100Hz using
120 the Cobra Probe (Watkins et al., 2002) which was mounted in the simulator.



121

122 *Figure 1: (a) Geometry of the University of Birmingham Tornado Vortex Generator (b) Dimensions of the*
123 *convergence chamber (c) Computational domain and boundary conditions.*

124 2.2 SWIRL RATIO

125 Whilst there are some variations for the definitions of swirl ratio in most laboratory studies (Monji,
126 1985, Mishra et al., 2008, Matsui and Tamura, 2009, Tari et al., 2010 and Gillmeier et al., 2017) and
127 numerical studies (Wilson and Rotunno, 1986, and Ishihara et al., 2011 and Ishihara and Liu, 2014),

128 the swirl ratio has generally been defined as the measure of intensity of the circulation of a vortex,
 129 while also describing the evolution of the stages of a tornado; from single-celled to multi-celled vortex.
 130 The swirl ratio, S used in the current research has been defined as:

$$S = \frac{\tan\theta}{2a} \quad [1]$$

131 where θ is the guide vanes angles and a is the aspect ratio, defined as:

$$a = \frac{2h_2}{D_3} \quad [2]$$

132 The definition of the aspect ratio is based on the physical dimensions of the simulator; the ratio
 133 between the diameter of the exhaust outlet (D_3) and the height of the inlet (h_2). The UoB-TVG has a
 134 fixed aspect ratio of 2, while other large-scale tornado vortex simulators have adjustable aspect ratios
 135 such as the WindEEE dome (Refan and Hangan, 2018) with aspect ratio of 0.35 to 1, VorTECH (Tang et
 136 al., 2017) of 0.5 to 1 and ISU Tornado simulator (Gairola and Bitsuamlak, 2019) of 1.09 to 5.46.

137 2.3 NUMERICAL DETAILS

138 The Large-eddy simulation approach employed in the current research was first proposed by
 139 Smagorinsky (1963); the LES uses sufficiently small grid resolution to directly compute the larger
 140 eddies in a turbulent flow, while the smaller unresolved scales of the turbulence were filtered and
 141 modelled via the sub-grid scale (SGS). Studies by Natarajan (2011), Maruyama (2011), Ishihara et al.
 142 (2011) and Ishihara and Liu (2014) found that the vortex core contains complicated turbulent flows
 143 and thus ideally suited to an LES. The open source CFD program OpenFOAM (OpenFOAM, 2019) was
 144 used to perform the LES with the assumption that the flow was incompressible and Newtonian in
 145 nature. The continuity and momentum equations were filtered as follows in order to obtain the
 146 governing equations:

$$\frac{\partial \bar{U}_i}{\partial x_i} = 0 \quad [3]$$

$$\frac{\partial \bar{U}_i}{\partial t} + \frac{\partial \bar{U}_i \bar{U}_j}{\partial x_j} = -\frac{\partial \bar{P}}{\partial x_i} + 2 \frac{\partial}{\partial x_j} (v + v_{sgs}) \bar{S}_{ij} \quad [4]$$

147 where U is the velocity field, t is the time and v is the kinematic viscosity. The spatial filtering operation
 148 for the LES is denoted by the bar over the physical quantities. The pressure (P) and filtered strain rate
 149 tensor (\bar{S}_{ij}) are expressed as:

$$\bar{P} = \frac{\bar{p}}{p} + \frac{(\overline{U_i U_j} - \bar{U}_i \bar{U}_j)}{3} \quad [5]$$

$$\bar{S}_{ij} = \frac{1}{2} \left(\frac{\partial \bar{U}_j}{\partial x_i} + \frac{\partial \bar{U}_i}{\partial x_j} \right) \quad [6]$$

150 The Smagorinsky model (Smagorinsky, 1963), was used to model the eddy viscosity under the effects
 151 sub-grid scale, v_{sgs} with the eddy viscosity coefficient as:

$$v_{sgs} = (C_s f_d \Delta)^2 \sqrt{2 \bar{S}_{ij} \bar{S}_{ij}} \quad [7]$$

152 where f_d is the damping function, Δ is the length scale of the SGS turbulence and C_s is the model
 153 coefficient, set to 0.1. The Van Driest type damping function (Van Driest, 1956) was employed in this
 154 study to calculate f_d and is expressed as:

$$f_d = 1 - \exp\left(\frac{-y^+}{25}\right) \quad [8]$$

155 where y^+ is the non-dimensional distance to the wall, depicted as the relationship between friction
 156 velocity and kinematic viscosity.

157 2.4 COMPUTATIONAL DOMAIN AND BOUNDARY CONDITIONS

158 The computational domain was created based on the configurations of the UoB-TVG, which was
 159 geometrically similar to the study by Gillmeier et al. (2017) as illustrated in figure 1. The convection
 160 chamber was simplified to a cylinder configuration for the convenience of grid generation. A cartesian
 161 coordinate system has been adopted for the generation of the computational domain, where the xy
 162 plane represents the horizontal plane while z axis represents the axis perpendicular to the horizontal
 163 plane. The flow enters the convergence chamber with a uniform velocity of $U_\infty=0.66$ m/s. The exhaust
 164 outlet was set with pressure outlet with the free stream pressure, $P_\infty=0$. A no-slip boundary condition
 165 was applied to the ground, surface walls of the guide vanes and the walls of the convection region.
 166 The results presented in this study were normalized using the characteristic parameters of the vortex:
 167 the maximum tangential velocity (U_T), the radius of the core (r_c) and time per revolution of the vortex
 168 (t_r). The method of determining the location of maximum tangential velocity and the radius of the core
 169 are presented in section 3.2, while the time taken for the vortex to complete a single revolution is
 170 defined as:

$$t_r = \frac{2\pi r_T}{U_T} \quad [9]$$

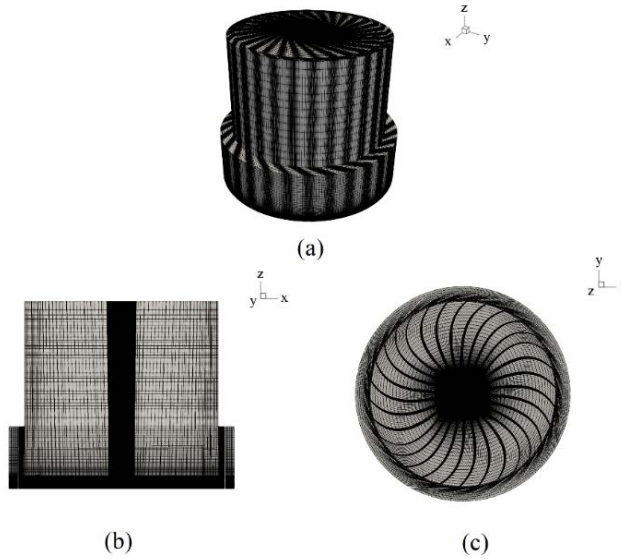
171 where r_T is the radial distance of the maximum tangential velocity. The pressure coefficient, C_p , is a
 172 non-dimensional parameter defined as:

$$C_p = \frac{P - P_\infty}{0.5 \rho_a U_T^2} \quad [10]$$

173 and ρ_a is the density of the air. The simulation was initialised with the inlet velocity, U_∞ . A second
 174 order implicit backward scheme was used to approximate the time discretization. The gradients were
 175 discretized with the second order central differencing scheme and the implicit PISO solver was used.
 176 (OpenFOAM, 2019). A constant time-step of $\Delta t= 5 \times 10^{-4}$ s was used throughout the entire transient
 177 simulation; this time-step was chosen to maintain the Courant-Friederichs-Lewy number (Courant et
 178 al., 1928) at the value less than 1 at every time step. The averaging of pressure and velocity were
 179 implemented when the vortex flow was fully developed, this was conducted by monitoring the
 180 residuals of each turbulent equation for convergence which ensured that the statistics did not change
 181 with time. Time time-averaged results were obtained by averaging the actual simulation time of 30
 182 seconds, which is equivalent to 300 vortex revolutions.

183 **2.5 MESHING**

184 ICEM-CFD (ICEM, 2012) mesh generator package was used to generate quadrilateral structured mesh.
 185 In order to resolve the boundary layer around the viscous sub-layers, 20 layers of mesh were created
 186 with the wall-adjacent spatial unit of $z^+ = 1$. Due to the axisymmetric structure of the tornado-like
 187 vortex, a clustered mesh with high density was adopted at the centre of the convergence chamber
 188 within the radius of 0.6 m from the centre, resulting in $x^+ \approx 10$ and $y^+ \approx 10$ in the tangential and radial
 189 directions. Hyperbolic stretching was used to generate the remaining meshes to ensure smooth
 190 transition. The mesh resolution around the guide vane regions in the convergence chamber were
 191 adjusted for the generation of three different mesh resolutions - coarse, medium and fine mesh with
 192 4 million, 7 million and 9 million cells respectively. The configuration of the generated mesh is shown
 193 in figure 2. Whilst every effort has been made to accurately reproduce the physical simulator there
 194 will inevitably be small differences introduced due to the meshing process. It is difficult to quantify
 195 the impact of these differences, but in what follows it is assumed that beyond a certain mesh
 196 resolution their effects are negligible (see section 3).



197
 198 *Figure 2: Mesh of the computational domain: (a) Isometric view (b) Side view) (c) Top view.*

199 **2.6 COMPUTATION FOR FLYING DEBRIS**

200 The three-dimensional motion of the debris in the tornado-like vortex was numerically computed.
 201 Each individual debris was assumed to be a three dimensional spherical compact object which did not
 202 undergo rotation. The Tachikawa number (Tachikawa, 1983) used in the current research is defined
 203 as:

$$K = \frac{\rho_a U_\infty^2 d^2}{2m_d g} \quad [11]$$

204 where ρ_a is the density of the air, U_∞ is the inlet velocity, d is the diameter of the debris, m_d is the
 205 mass of the debris and g is the acceleration due to gravity. The Tachikawa number K , describes the
 206 ratio between the aerodynamic forces to the gravitational force, therefore, debris with lower mass
 207 will have higher value of K and are in theory, prone to fly higher and further. Properties of the debris
 208 considered in the current study were shown in table 1.

Table 1: Properties of the debris groups

Debris group	K	Diameter (m)	Density (kg/m ³)	Mass (kg)
A	2.5	0.00075	28.1	6×10^{-9}
B1	1.2	0.0015	28.1	50×10^{-9}
B2	1.2	0.00075	56.2	12×10^{-9}
B3	1.2	0.00037	112.4	3×10^{-9}
C	0.6	0.003	28.1	397×10^{-9}

210 The trajectories of the debris were computed using the transient solver
 211 icoUncoupledKinematicParcelFoam (OpenFOAM, 2019), where the motion was solved by considering
 212 the particle equilibrium using the Lagrangian frame of reference on the established flow field. Since
 213 the size of the largest debris considered (debris group C) was $\sim 10^8$ times smaller than the convergence
 214 chamber, the effects of debris on the flow were considered to be negligible. Hence, a one-way
 215 coupling was assumed to be sufficient, where debris were treated as point mass and generalized by:

$$\frac{ds_d}{dt} = U_d \quad [12]$$

$$m_d \frac{dU_d}{dt} = F_{total} \quad [13]$$

216 where s_d is the spatial position of the debris, U_d is the debris velocity, and F_{total} as the sum of all forces.
 217 The relevant forces acting on the particle were:

$$F_{total} = F_D + F_G \quad [14]$$

218 where F_D is the drag force and F_G is the gravitational force. These forces represent the dominant forces
 219 acting of the debris, while other forces were neglected. The drag force is expressed as:

$$F_D = \frac{3}{4} \frac{\rho_a m_d}{\rho_d d} \cdot C_D (U - U_d) |U - U_d| \quad [15]$$

220 where U is the velocity of the local flow field, and C_D is the spherical drag coefficient that is computed
 221 based on the debris Reynolds number (Putnam, 1961) as:

$$C_D = \begin{cases} \frac{24}{Re_d} \left(1 + \frac{1}{6} Re_d^{\frac{2}{3}}\right), & Re_d \leq 1000 \\ 0.424, & Re_d > 1000 \end{cases} \quad [16]$$

222

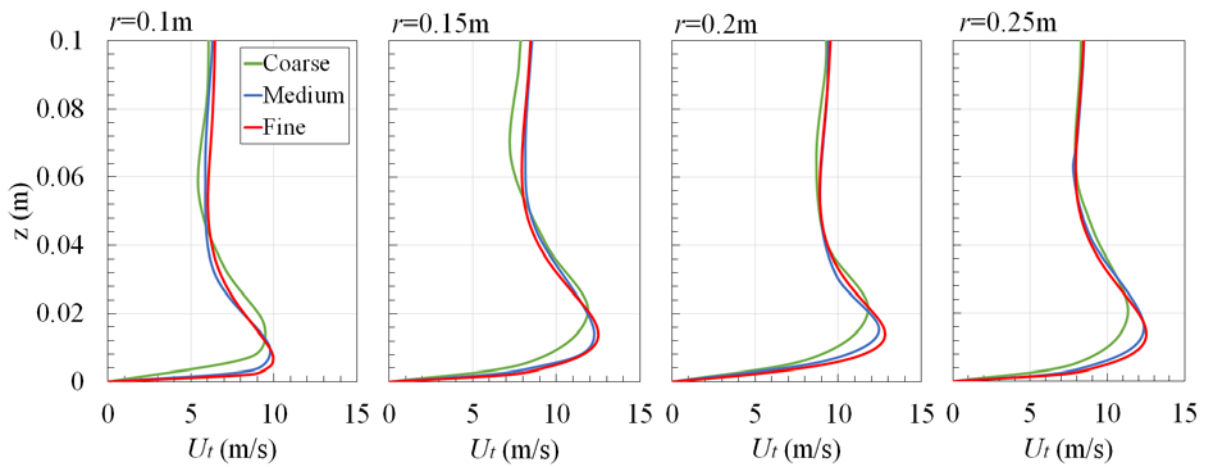
$$Re_d = \frac{\rho_a U d}{\mu_a} \quad [17]$$

223 where μ_a is the viscosity of air. Each debris group was simulated for 50 time instances in the flow. At
 224 each time step, 9 debris were placed at different radial positions on the ground to be initialized by the
 225 flow, at 0m, 0.0275m, 0.55m, 0.0825m, 0.11m, 0.165m, 0.22m, 0.275m and 0.33m. A total of 2250
 226 debris were released in the flow field.

227 **3. RESULTS FOR THE TORNADO-LIKE VORTEX**

228 **3.1. ASSESMENT OF NUMERICAL ACCURACY**

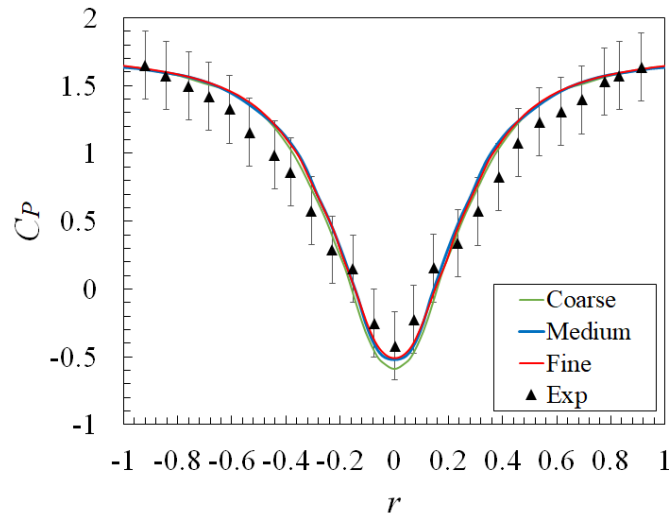
229 In order to investigate the impact of grid resolution on the numerical results, computations were
230 conducted on three mesh resolutions- coarse, medium and fine meshes. The velocity components U_t ,
231 U_r and U_v represents the tangential, radial and vertical velocities respectively. Due to the axis-
232 symmetrical structure of the vortex, horizontal positions from the centre were expressed using the
233 radial distance, r . Figure 3 shows the comparison of vertical distribution of time averaged tangential
234 velocity extracted from different locations, $r=0.1, 0.15, 0.2$ and $0.25m$. At all radial positions, the
235 coarse, medium and fine meshes show similar trends with respect to the vertical distribution of the
236 tangential velocity, with the medium and fine meshes both predicted similar results. The maximum
237 tangential velocities obtained from the three meshes are 11.7, 12.4 and 12.5 m/s for coarse, medium
238 and fine meshes, respectively.



239

240

Figure 3: Vertical profiles of time averaged tangential velocity at the position $r/r_c = 1, 1.5, 2$ and 2.5 .



241

242

243

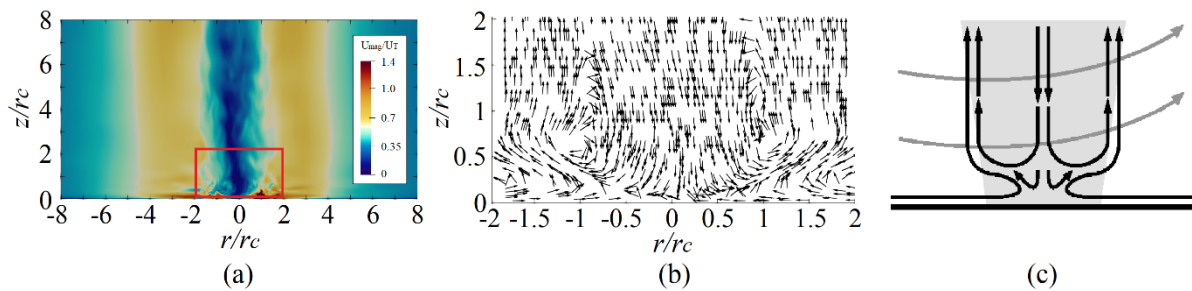
Figure 4: Distribution of time averaged pressure coefficient on the ground surface in comparison with experimental data Gillmeier et al. (2017).

244 The experimental results of Gillmeier et al. (2017) were used as a comparison for the numerical
245 simulation. It is worth noting that experimental velocity and pressure data have an uncertainty of \pm
246 2% and \pm 0.5%. Figure 4 illustrates the agreement between the numerical simulations and
247 experimental data in terms of surface pressure coefficient. For all meshes it can be observed that the

248 data from LES agrees well in terms of magnitude and trend with the experimental data. (A comparison
249 using the velocity measurements is presented later in section 3.2 and shows a similar level of
250 agreement with the medium mesh.)

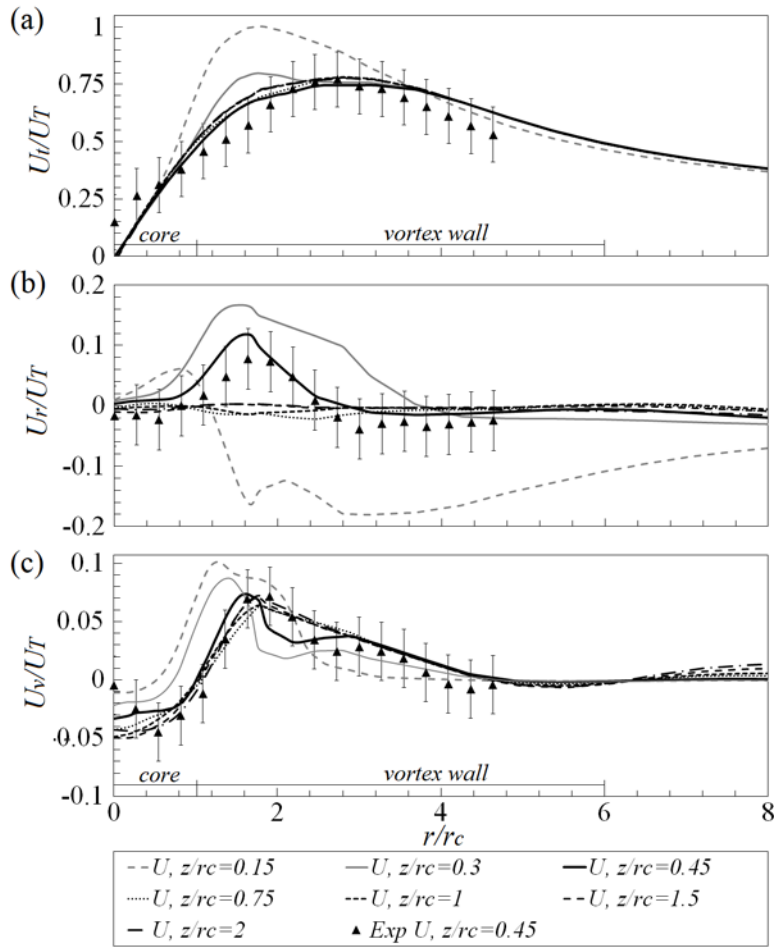
251 3.2 FLOW FIELD

252 The results from the numerical simulation of a tornado-like vortex with the swirl ratio of 0.7 are
253 presented in this section. The flow features of the vortex structure were analysed and the method of
254 determining the radius of the core and vortex wall thickness are discussed. Figure 5 illustrates the
255 contours of instantaneous velocity magnitude and the vectors of averaged radial and vertical velocity,
256 where U_{mag} denotes the velocity magnitude of the flow field. The tornado-like vortex consists of two
257 main features, a vortex core and thick vortex walls. The core is situated at the centre of the vortex
258 while the wall surrounds the core and gives an outline to the structure of the vortex. The vortex was
259 observed to exhibit a very minor and random wandering motion where the core shifts at the maximum
260 distance of approximately $r/r_c=0.18$ from the centre axis. Based on the velocity vectors, the centre of
261 the vortex consists of downwards flow - a region of inflow was observed towards the centre, and then
262 redirects towards the vertical direction. The radial distance in which separates the upwards and
263 downwards flow was identified as the core radius.



264

265 *Figure 5: (a) Contours of instantaneous velocity magnitude of tornado-like vortex (b) Averaged radial and*
266 *vertical velocity vector of the regions in the red box (c) Sketch of the tornado-like vortex to illustrate the flow*
267 *structure.*



268

269 *Figure 6: Horizontal profiles of time averaged velocity components at different elevation in comparison with*
 270 *experimental results (Exp) by Gillmeier et al. (2017).*

271 Figure 6 shows the horizontal profiles of time averaged velocities extracted from the flow fields at the
 272 elevations of $z/r_c = 0.15, 0.3, 0.45, 0.75, 1, 1.5$ and 2 . The experimental results by Gillmeier et al. (2017)
 273 were ensemble averages used as a comparison for the numerical simulation; data shown in the figure
 274 corresponds to the elevation of $z/r_c = 0.45$ (where r_c is the core radius). The maximum tangential
 275 velocity of the vortex, U_T was 12.53 m/s and occurs at the radial distance, r_T of 1.82 ($r/r_c = 1.82$) at the
 276 elevation of $z/r_c = 0.15$; the velocity U_T was used as a characteristic velocity, as shown in figure 6(a).

277 The time per revolution of the vortex, t_r was calculated based on r_T and U_T , revealing the vortex to be
 278 approximately 0.1 seconds per revolution. The normalised radius of the core ($r/r_c = 1$, where $r_c = 0.11$ m)
 279 was calculated based on the averaged radial distance with respect to height of the layer with zero
 280 vertical velocity, ($U_v/U_T = 0$) (as shown in figure 6(c)). The tangential velocity at r_c was $U_t/U_T = 0.48$, and
 281 was used to mark the boundaries of the vortex wall spanning from approximately $r/r_c = 1$ to 6 (as shown
 282 in figure 6(a)). As a result, the core at the centre of the vortex consists of low velocities, while high
 283 velocity magnitudes surround the core within the vortex wall.

284 In general, apart from the profile of $z/r_c = 0.15$, the distribution of tangential velocity shows a similar
 285 trend and magnitude at all elevations. In figure 6(b), the profile at $z/r_c = 0.15$ shows an outwards flow
 286 from the centre of the vortex to the radial distance of $r/r_c = 1.2$ and then changes to inflow as the radial
 287 distance increases. Low magnitudes of radial velocity components were observed at higher elevations.
 288 Based on the profiles of vertical velocities in figure 6(c), a similar distribution can be observed at all
 289 elevations, with negative velocities at the centre of the vortex and increasing to maximum magnitude

290 between $r/r_c=1.5$ to 1.8. Some minor differences can be observed around the core region between
291 $r/r_c=0$ to 2, where the experimental results have the highest uncertainties. Overall, the predicted
292 velocity field matches that given by the physical results. However, both the numerical and physical
293 simulations are not without their limitations: accurately specifying inflow boundary conditions are
294 crucial for LES yet fraught potentially with difficulties (Yang, 2015), as very specific information on
295 turbulence is required to reproduce identical inflows, e.g., turbulence intensity, stochastically varying
296 turbulent length scales, and power spectrums of turbulent etc. The effects of sub-grid scale (SGS)
297 modelling is also considered to be a potential source of uncertainty since SGS motions inevitably
298 requires unrealistically fine cells at all regions even locations far away from the vortex structure.
299 Notwithstanding these limitations, the numerical results presented in the paper are within the range
300 of experimental uncertainty and considered suitable for the purposes of this work.

301 **4 RESULTS FOR DEBRIS FLIGHT**

302 The results for the simulation of debris flight using the flow field outlined in section 3.2 are presented
303 in this section. In all cases, the results have been normalized with the parameters of U_T , r_c and t_r as
304 appropriate. Debris group A, B1, B2, B3 and C (presented in table 1) were simulated at 50 different
305 time instances respectively; the release times were chosen at every quarter revolution of the vortex,
306 ($t_r \approx 0.025s$). A total of 2250 individual debris groups were released from 9 different locations in the
307 flow; 5 locations within the core of the vortex at $r/r_c=0, 0.25, 0.5, 0.75$ and 4 locations away from the
308 core at $r/r_c=1.5, 2, 2.5$ and 3. Results from the simulation of debris group B1, B2 and B3 with identical
309 Tachikawa number of $K=1.2$ were compared for the aerodynamic similarity in section 4.1, while
310 section 4.2 investigates the behaviour of debris with varying Tachikawa number of $K=2.5, 1.2$ and 0.6
311 for debris group A, B1 and C respectively.

312 **4.1 RESULTS FOR DEBRIS B1, B2 AND B3 (K =1.2)**

313 The distribution of flight duration of all released debris are shown in figure 7 and expressed in terms
314 of the flight duration of each individual debris, t_d , normalized by the revolution of the vortex, t_r . The
315 flight duration was calculated based on the total airtime of debris from initialization to the impact on
316 the ground surface, where the maximum and minimum flight durations are represented by the
317 whiskers on the box plots. It can be observed that all 3 debris types show similar interquartile range
318 with positive skew; the mean flight duration (denoted by a "x") was approximately $t_d/t_r \approx 4$ in all cases.
319 Debris that were not initialized or had a flight duration of less than a single revolution, (i.e., $t_d/t_r < 1$)
320 were not considered as wind-borne in the current analysis; as a result, the total number of wind-borne
321 debris for debris group B1, B2 and B3 were 90, 82 and 86 respectively (20%, 18% and 19% for debris
322 group B1, B2 and B3 respectively). The low percentage of windborne debris were not too surprising
323 as this study focuses only on the wind-borne behaviour in a stationary tornado, where the translation
324 effects of the tornado were ignored. However, it is worth nothing that the translational movement of
325 a naturally occurring tornado could potentially result in higher percentage of debris becoming wind-
326 borne; several researches (Kosiba et al., 2014; Matsui et al., 2008; Phuc et al., 2012) have been carried
327 out where the translating speed of tornado ranges from $0.05 U_T$ to $0.7 U_T$.

328 Figure 8 illustrates the plan view of the trajectories of wind-borne debris for debris group B1, B2 and
329 B3 that were initialized from the locations of $r/r_c=0.5, 0.75, 1, 1.5$ and 2. Data pertaining to the
330 locations $r/r_c=0, 0.25, 2.5$ and 3 are not shown since debris flight initialized from these locations was
331 infrequent, largely due to the downwards flow at the centre of the vortex region ($r/r_c=0$ and 0.25) and
332 the absence of updraft flow at regions further from the core ($r/r_c=2.5$ and 3). In general, the
333 trajectories of all debris from group B show a very similar path distribution at all locations, although
334 debris initialized from the location $r/r_c=0.5$ tends to show a greater degree of variation in trajectory.

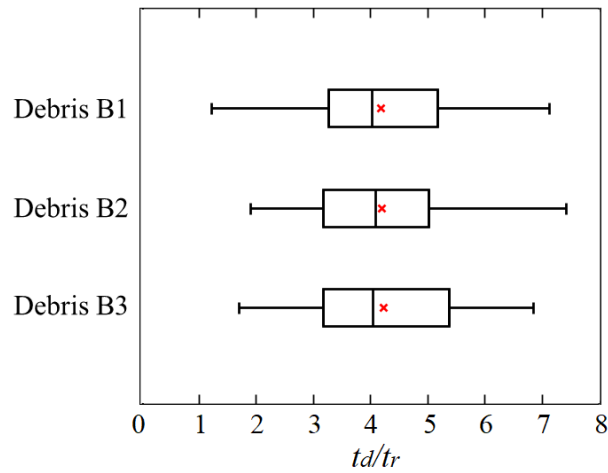


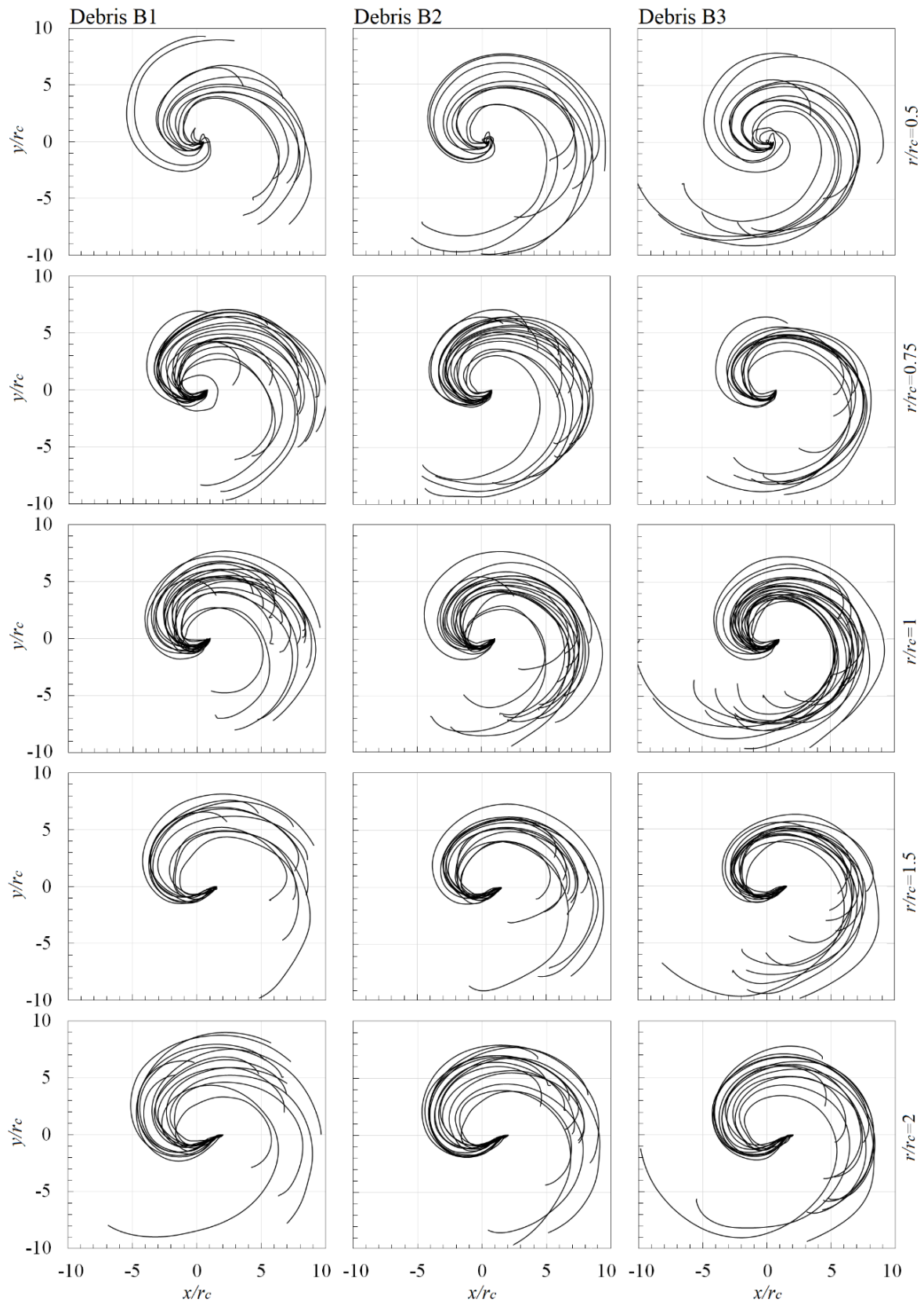
Figure 7: The distribution of flight duration of debris group B1, B2 and B3

335

336

337 The results from the experimental research conducted by Bourriez et al. (2017) were used as a
 338 comparison. The experimental study investigates the flight behaviour and motion of wind-borne
 339 debris in the tornado-like vortex at the swirl ratio of $S=0.7$. The debris used in the experiments were
 340 spherical polystyrene beads with varying diameter of 1.5 – 1.7 mm and densities of 24-28 kg/m^3 , and
 341 corresponds to debris group B1 used in the simulation. The motion of the debris were tracked using
 342 the 3D-PTV technique (Maas et al., 1993; Malik et al., 1993). Two high speed digital cameras (Sony
 343 NEX-FS700RH) were positioned in the simulator and setup to record videos at 480 fps with the
 344 resolution of 1920 x 1080 pixels (confines of the tracking window not specified). Variations in results
 345 were found due to the relatively inconsistent size of the debris used, and the considerable changes on
 346 the local field of the vortex due to the wandering motion or turbulent fluctuations. Figure 9 shows the
 347 comparison of debris trajectories from numerical simulation and experimental results. The locations
 348 of $r/r_c=1$ and 2 corresponds to the closest release position from the experiments at $r/r_c \approx 0.9$ (100mm)
 349 and $r/r_c \approx 1.8$ (200mm).

350 The trajectories of the wind-borne debris were represented in black solid lines for the results from
 351 numerical simulation and the grey lines from the experiments while the red solid lines represents
 352 the mean trajectory of the numerical simulation and red dashed lines represents the mean
 353 trajectory of the experimental results.

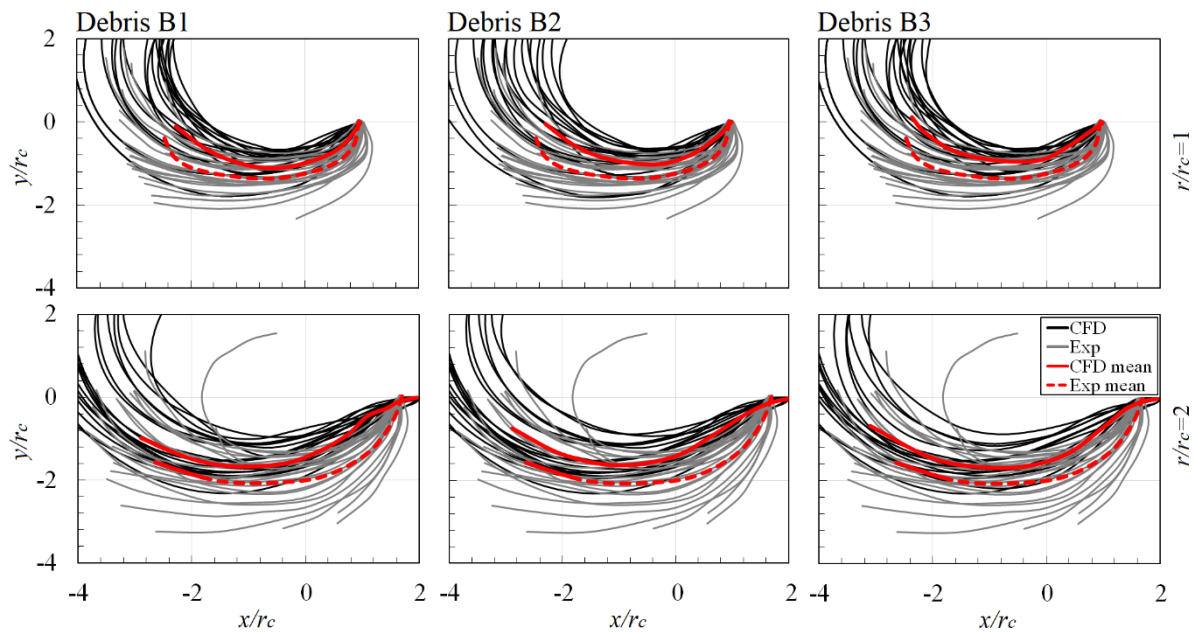


354

355
356

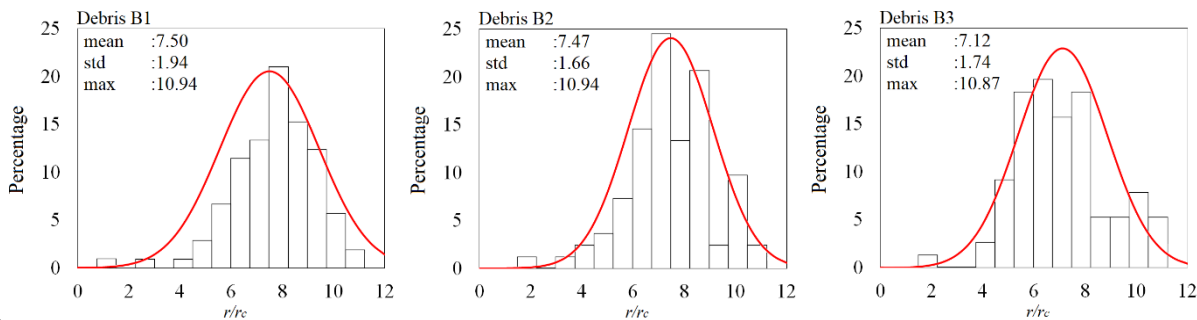
Figure 8: Plan view of debris trajectories at the locations of $r/r_c=0.5, 0.75, 1, 1.5$ and 2 for debris group B1, B2 and B3.

357 All three debris groups predicted similar distributions of debris trajectories at both release positions,
 358 while the debris trajectories from the experimental results shows shorter trajectories in comparison
 359 with the numerical simulation as debris left the tracking window and the entire trajectories were not
 360 captured. Both the numerical and experimental results corresponds well (considering the uncertainty
 361 associated with the results) at the location $r/r_c=1$ with the overlapping trajectory path of
 362 approximately 78%; while at the location $r/r_c=2$, the overlapping region was lower at approximately
 363 61%; the numerical simulation predicted trajectories that were closer to the vortex core while the
 364 experiment shows trajectories that were further from the core. The mean trajectories of both the
 365 experiments and numerical simulations shows very similar curvature with the distance of
 366 approximately $r/r_c=0.4$ apart; this is likely due to the larger variation in the trajectory paths from the
 367 experiments, caused by the turbulent fluctuation in the local field.



368

369 *Figure 9: A close-up view of debris trajectories at the locations of $r/r_c=1$ and 2 for debris group B1, B2 and B3*
 370 *in comparison with experimental data from Bourriez et. al (2017).*



371

372 *Figure 10: The distribution of impact radius of all released debris based on debris group, with mean, standard*
 373 *deviation and maximum values.*

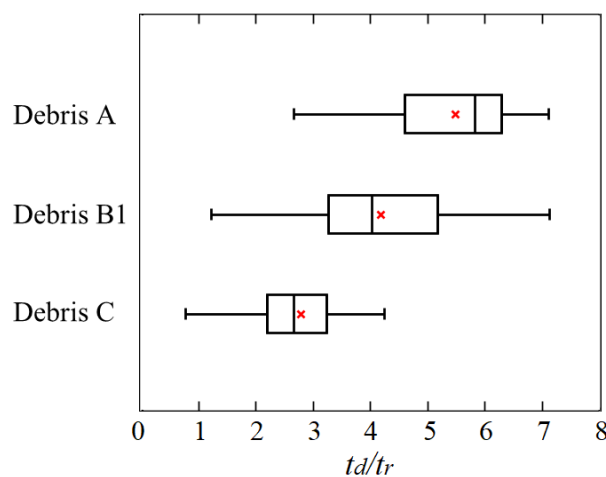
374 In figure 10, the bar chart shows the distribution of impact radius while the curve (red line)
 375 corresponds to the normal distribution of all wind-borne debris, expressed in terms of the percentage
 376 of occurrence against the impact radius. The distance between the impact locations and the centre of
 377 the vortex was expressed as the impact radius as this provides a measurement of damage range for
 378 the tornado-like vortex, while the percentage was calculated based on the number of occurrence for

379 wind-borne debris that impacts at that respective radial distance. The mean impact radius for debris
 380 group B1, B2, and B3 were 7.5, 7.5 and 7.1 respectively. Due to high magnitudes of velocity
 381 components between $r/r_c=0$ to 3, a sparse distribution of debris impact was observed around that
 382 region. A clustered distribution of debris impact can be seen around the edge of the vortex walls that
 383 is further away from the core ($r/r_c > 6$), where velocity magnitudes were low.

384 The aerodynamic similarity of debris group B1, B2 and B3 was examined. Understandably, all 3 debris
 385 groups were shown to exhibit the propensity to travel with very similar flight duration and trajectories
 386 due to the identical value of Tachikawa number. In general, the prediction of debris trajectories
 387 corresponds well for both the numerical simulation and experiments results; however, it should be
 388 pointed out that debris were assumed to be one-way coupled and the motion of debris were also
 389 assumed with no rotation in a highly swirling flow, which may result in some difference in overall
 390 trajectories between numerical and physical simulation. We also note the lack of turbulence data
 391 associated with the physical measurements results in an uncertainty of the flow simulation in this
 392 region. Notwithstanding this the numerical simulation are consistent with the physical data and able
 393 to capture the entire flight duration from initialization to the impact on the ground. Furthermore, the
 394 numerical simulations provide a better understanding of the impact distribution and extend the
 395 results of the physical simulation.

396 **4.2 RESULTS FOR DEBRIS A, B1 AND C (K = 2.5, 1.2 AND 0.6 RESPECTIVELY)**

397 In this section, the behaviour of wind-borne debris in tornado-like vortex with varying Tachikawa
 398 number (0.6 – 2.5) was studied. The distribution of flight duration for all released debris are shown in
 399 figure 11, expressed in terms of the flight duration of each individual debris, t_d , normalized by the
 400 revolution of the vortex, t_r . The flight duration was calculated based on the total airtime of debris from
 401 initialization to the impact on the ground surface, where the maximum and minimum flight durations
 402 are represented by the whiskers on the box plots. Debris that were not initialized or had a flight
 403 duration of less than a single revolution, $t_d/t_r < 1$ were not considered as wind-borne. As a result, the
 404 total number of wind-borne debris for debris group A, B1 and C was 122, 90 and 54 respectively (27%,
 405 20% and 12% for debris group A, B1 and C respectively). The Tachikawa number is a ratio of
 406 aerodynamic forces relative to gravitational force of a wind-borne debris, therefore, light debris (low
 407 mass) with high values of K will have the tendency to stay airborne for longer. Hence, the mean flight
 408 duration (red "x") for all 3 debris groups were considerably different; the smaller and lighter debris A
 409 has significantly longer flight duration than the heavier and larger debris C. The mean flight duration
 410 for debris group A, B1 and C were $t_d/t_r=5.49$, 4.19 and 2.79 respectively.



411

412

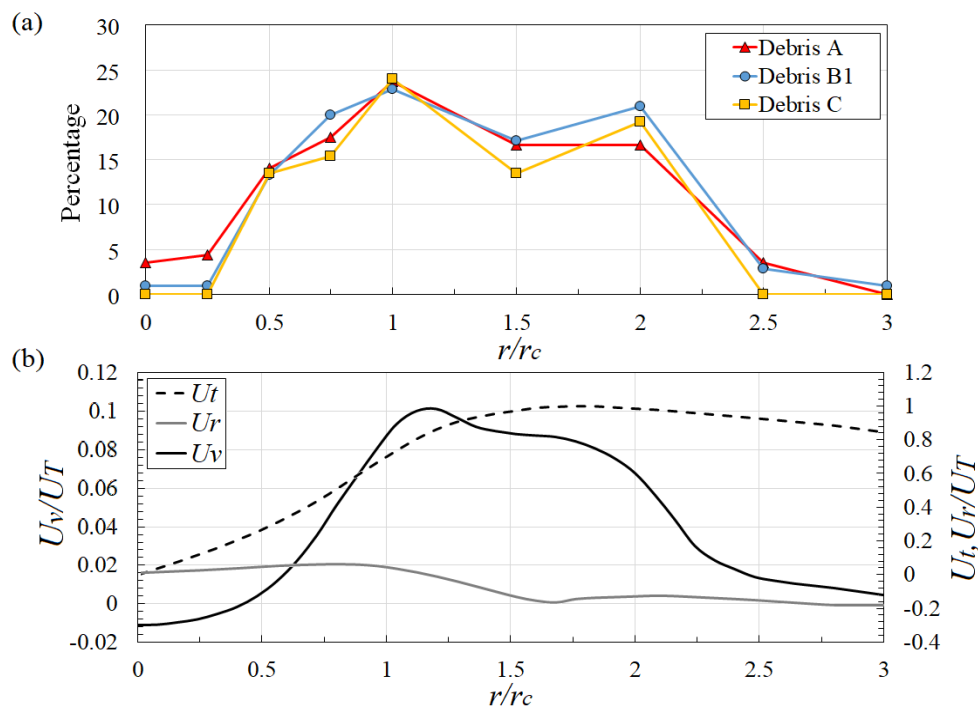
Figure 11: The distribution of flight duration of debris group A, B1 and C.

413 Figure 12(a) shows the percentage of wind-borne debris that were initialized by the vortex at different
414 radial positions. The percentage was calculated based on the number of debris that were initialized
415 by the vortex at that position with respect to the total number of wind-borne debris (122, 90 and 54
416 debris for debris group A, B1 and C respectively). Hence, at the location $r/r_c=1$, 30 individual debris
417 particles from group A were initialized yielding 24%, while 13 individual debris of debris group C were
418 initialized yielding 24%. Figure 12(b) shows the horizontal profiles of tangential, radial and vertical
419 velocity components that corresponds to the debris release positions. The scales of the normalized
420 vertical velocity are shown on the left vertical axis while the normalized tangential and radial velocity
421 are shown on the right vertical axis. This was done to highlight the distribution of vertical profile
422 without being overshadowed by the high magnitudes of tangential velocity. As discussed earlier, the
423 centre of the vortex primarily consists of downwards flow, while maximum magnitude of updraft flow
424 can be found around the vortex core region, $r/r_c=1$. A relatively high magnitude of tangential velocity
425 is present at the region $r/r_c>1$. Based on the figure, it can be observed that the percentage distribution
426 of debris initialization based on the position shows a correlation with the vertical velocity profile.
427 Furthermore, all three debris groups illustrate similar trends with the highest percentage at the core
428 radius, $r/r_c=1$ despite the difference in total number of debris considered as wind-borne. Regions
429 further away at $r/r_c=2.5$ and $r/r_c=3$, and around the centre of the vortex at $r/r_c=0$ and $r/r_c=0.25$ were
430 observed to have a very low possibility of flight initiation by the flow despite the high magnitudes of
431 tangential and radial velocities. The increase of vertical flow from $r/r_c=0.5$ to $r/r_c=2$ resulted in the
432 increase in the percentage of debris initialization, where debris that were positioned around this
433 region were approximately 10% more likely to be initialized. This is due to the upwards lift produced
434 by the vertical velocity that provides the elevation for debris to become wind-borne. A small number
435 of particles appear to have become windborne for debris A and B at $r/r_c=0$. This is due to the wandering
436 motion of the vortex, where the core shifted approximately $r/r_c=0.18$ from the centre axis. Although
437 the shift is not significant, the radial outflow at the centre in addition with the absence of downward
438 flow provided sufficient condition for debris to become wind-borne.

439 Figure 13 illustrates the plan view of the trajectories of all wind-borne debris for debris group A, B1,
440 and C that were initialized from the position of $r/r_c=0.5, 0.75, 1, 1.5$ and 2 to the impact on the ground
441 surface. The positions of $r/r_c=0, 0.25, 2.5$ and 3 are not shown as debris initialized from those locations
442 was infrequent. The smaller debris (group A) were observed to have high variation in debris
443 trajectories at all positions and the longest average flight duration. In this case, the debris were
444 observed to circulate around the vortex core, resulting in long and scattered trajectories. On the
445 contrary, the trajectories for the larger debris group C shows lower curvature and does not have the
446 tendency to circulate around the vortex. In general, the distribution of trajectories for each respective
447 debris group shows similar variation at every position.

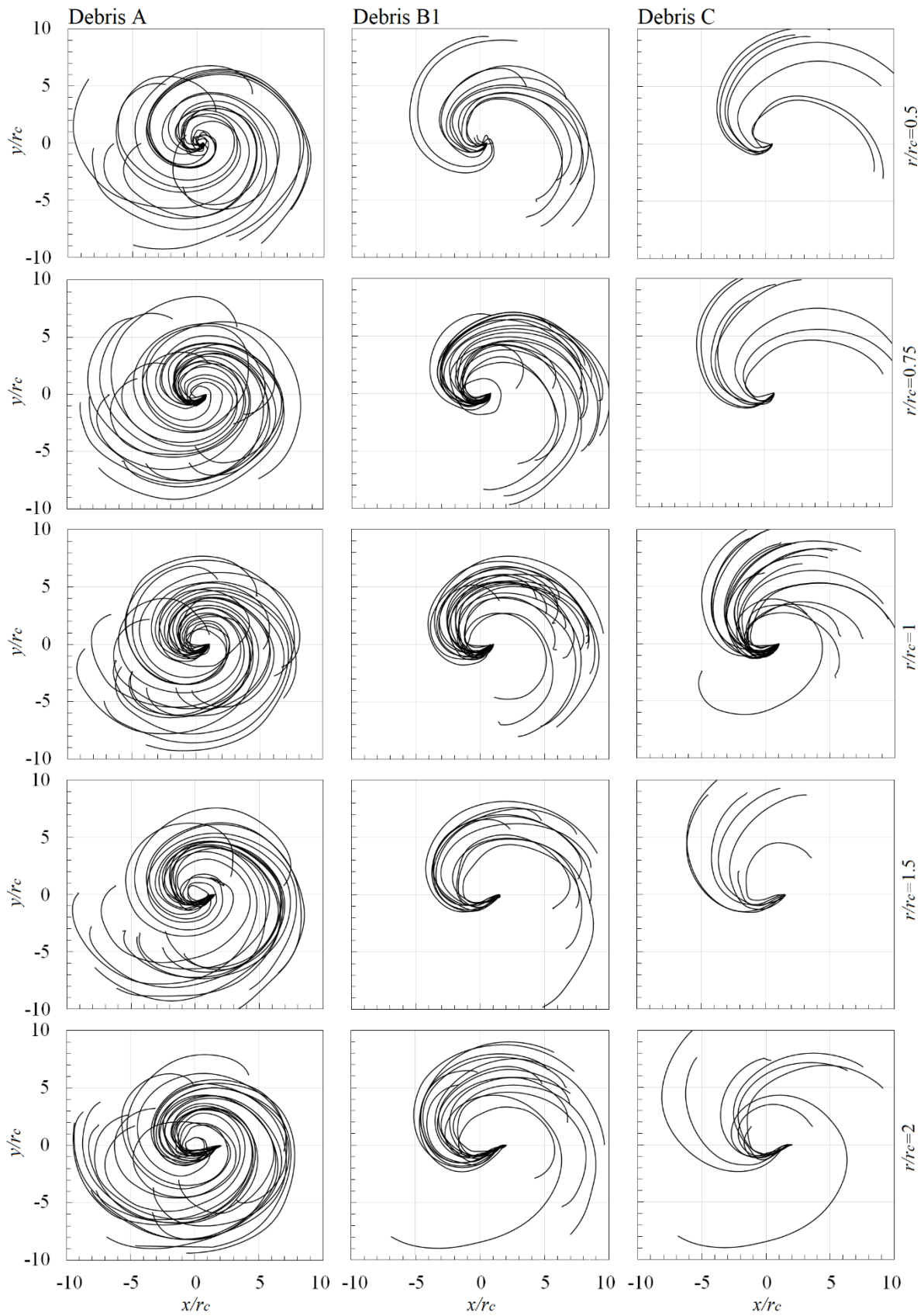
448 In figure 14, the bar chart shows the distribution of impact radius while the curve (red line)
449 corresponds to the normal distribution of all wind-borne debris, expressed in terms of the percentage
450 of occurrence against the impact radius. The percentage was calculated based on the number of
451 occurrences of wind-borne debris that impacted at that respective radial distance. A different range
452 of impact radii were observed for groups A, B1 and C: debris A shows the shortest mean impact radius
453 of $r/r_c \sim 7.0$, whilst debris C has the greatest impact radius of $r/r_c \sim 9.0$. Concurrently, debris C exhibited
454 the highest impact potential with a maximum value of $r/r_c = \sim 12.0$, whereas debris A and B shows
455 comparable maximum impact radii of $r/r_c \sim 11.0$. The normal distribution suggests similar variation for
456 all debris, with the standard deviation for each group ~ 2.0 . Although the smaller and lighter debris A
457 has longer flight duration, it does not impact at greater radial distance from the vortex; this
458 phenomenon will be discussed and shown in figure 15.

459 Figure 15 shows the total flight duration of each individual wind-borne debris from initialization to the
 460 impact on the ground against the radial distance from the centre of the vortex throughout the flight.
 461 Thus, providing an insight to the debris trajectories in relation to the regions of the vortex whilst also
 462 characterising the behaviour of different debris groups. All debris shows a reduction in radial distance
 463 once initialized, indicating the tendency to travel towards the centre before for values of $t_d/t_r < 0.4$.
 464 For debris group A, the radial distance for the debris were observed to increase rapidly away from the
 465 centre after the flight time of $t_d/t_r > 0.4$; while some debris were ejected outwards with the radial
 466 distance of more than $r/r_c = 8$, the majority of the debris circulates around the region between $r/r_c=6$
 467 to 8 after the flight duration of $t_d/t_r = 2$. Towards the end of the flight duration, a decrease in radial
 468 distance was observed as the debris were drawn towards the vortex due to the radial inflow, as shown
 469 in figure 16.



470

471 Figure 12: (a) The percentage distribution of all wind-borne debris at the position of $r/r_c=0, 0.25, 0.5, 0.75, 1,$
 472 $1.5, 2, 2.5$ and 3 . (b) The horizontal profiles of tangential, radial and vertical velocities of the tornado-like vortex
 473 at the elevation of $z/r_c=0.015$.

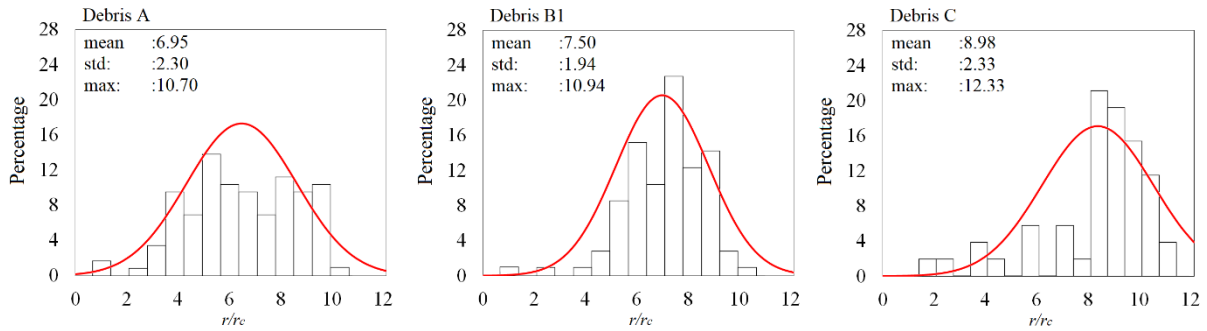


474

475

476

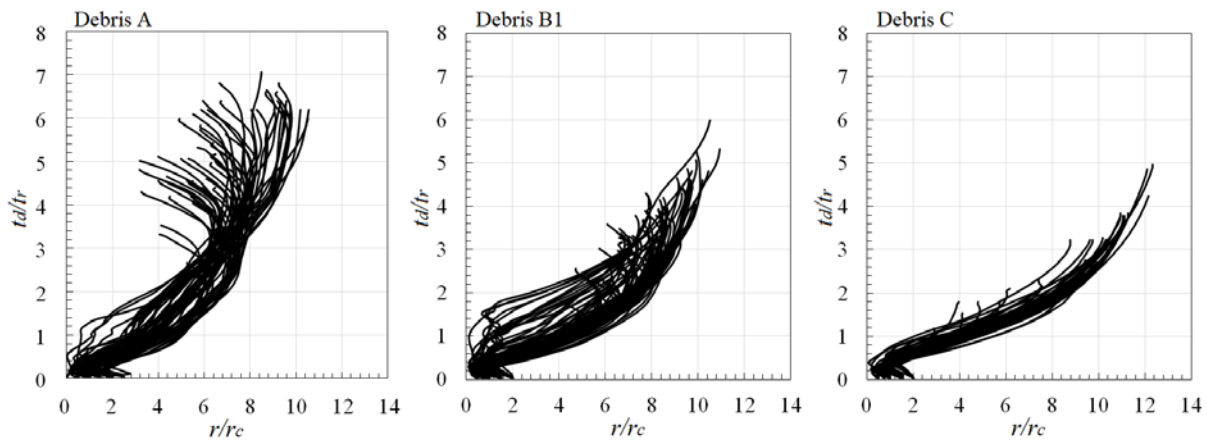
Figure 13: Plan view of debris trajectories at the locations of $r/r_c=0.5, 0.75, 1, 1.5$ and 2 for debris group A, B1 and C.



477

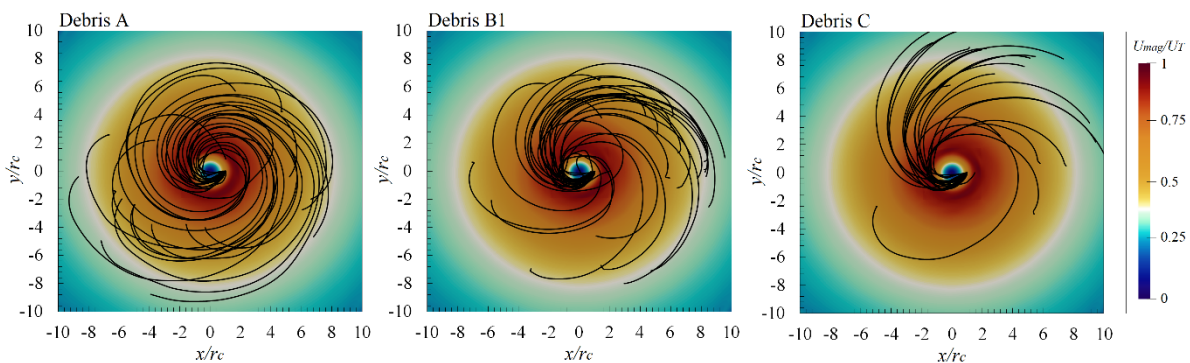
478 *Figure 14: The distribution of impact radius of all released debris based on debris group, with mean, standard*
 479 *deviation and maximum values.*

480 In general, the debris group A has approximately 60% of the flight duration around the vortex walls
 481 regions. On the contrary, the radial distance of debris group C were observed to constantly increase
 482 throughout the flight duration due to the inertia of the debris, travelling further away from the centre
 483 until the impact on the ground. The trajectories of debris group B exhibited a mixture of behaviours
 484 with some particles travelling beyond the vortex wall whilst others circulated close to walls.



485

486 *Figure 15: The flight duration of wind-borne debris against the radial distance from the centre of the vortex for*
 487 *debris group A, B1 and C.*



488

489 *Figure 16: The top view of debris trajectories at the location $r/r_c=1$ with the contours of averaged velocity*
 490 *magnitude for debris group A, B1 and C.*

491 The plan view of the trajectories of the debris initialized from the position $r/r_c=1$ with contours of
 492 normalized tangential velocity shown in figure 16. The red contours in figure 16 indicates the vortex
 493 walls. As discussed previously, the trajectories of debris group A are observed to circulate within the
 494 vortex wall between $r/r_c= 1$ to 6 with a tendency to be drawn back towards the core at end of the

495 flight duration. However, for debris group C it is clear that the vast majority of debris are ejected away
496 from the centre and out of the vortex walls.

497 5. CONCLUSIONS

498 The objective of this present research was to investigate the flight behaviour of different groups of
499 debris in a tornado-like wind field. Hence, large eddy simulations were undertaken for a tornado-like
500 vortex with a swirl ratio of 0.7. Acknowledging the uncertainty associated with the data, the numerical
501 simulations agree well with previous experimental research and provide a greater insight into the flow
502 field. The following conclusions can be made:

- 503 • The tornado-like vortex consists of two main features, a core and thick vortex wall around the
504 core. The vortex wall consists of high velocity magnitudes where the maximum velocity
505 components occurs around the near ground region.
- 506 • The aerodynamic behaviour for three groups with the same Tachikawa number (B1, B2 and
507 B3) shows very similar flight behaviour and trajectories. All three debris groups exhibit a mean
508 flight duration of $t_d/t_r \approx 4$ with an impact radius of $r/r_c \sim 7.5$.
- 509 • The aerodynamic behaviour for three groups with varying Tachikawa numbers (A, B1 and C)
510 demonstrated that debris group with a lower mass (A) has the highest percentage of wind-
511 borne particles (~27%) compared to 20% and 12% for debris group B1 and C respectively.
512 Group A also had a considerably longer flight duration ($t_d/t_r \sim 6.0$), than groups B and C with
513 $t_d/t_r \sim 4.0$ and 3.0 respectively. During debris initializing stage, the debris positioned at the
514 radial location of $r/r_c=1$ had the highest possibility of becoming wind-borne, whereas debris
515 positioned around the regions within the core at $r/r_c=0$ and 0.25 and at regions where $r/r_c >$
516 2.0 were less likely to be initialized. This was due to the higher vertical velocities around $r/r_c =$
517 1 which appear to be key to flight initiation.
- 518 • The distribution of trajectories for debris group A were found to be scattered with high
519 variation but low average impact range of $r/r_c=7.0$, whilst debris group C has trajectories with
520 a lower curvature but greater high radius ($r/r_c \sim 9.0$). Further analysis of the flight duration
521 indicated that debris group A had the tendency to circulate within the regions of vortex walls
522 with consistent radial distance from the centre, whereas for group C the radial distance was
523 observed to constantly increase until the particles impacted on the ground.
- 524 • Low mass debris with high values of K were prone to travel for longer flight duration but as
525 indicated above, tended to be trapped within the vortex walls. This has important implications
526 when considering the wind loading arising from wind borne debris as a result of tornadic
527 activity.

528 The flow field of the tornado-like vortex and the flight behaviour of different debris groups were
529 discussed in detail. It is worth noting that current study only considers the flow field of the vortex at
530 $S=0.7$. Different swirl ratios have the potential to result in different flow characteristics and those
531 would affect the overall behaviour of wind-borne trajectory. Further, the flight characteristics of
532 debris were assumed with no rotation, which might be considered less realistic in a highly swirling
533 vortex flow field when the rotation of debris generates lift, which would lead to a different interaction
534 between the fluid and debris. It is also worth noting that this work has simulated the flow assuming
535 one single definition of aspect ratio, but as indicated by Gillmeier et al. (2019) and Gairola and
536 Bitsuamlak (2019), this may be an important area which has hitherto largely been neglected.
537 Notwithstanding this, this research shows the flight behaviour of different debris groups and their
538 corresponding impact range and thus enables the potential dangers associated with flying debris in
539 tornadoes to be evaluated.

540 **Acknowledgements**

541 The authors would like to acknowledge the Birmingham Environment for Academic Research
542 (BlueBEAR) at the University of Birmingham for providing the software licenses and computational
543 resources.

544 **Reference**

- 545 [1]. Alexander, C.R., Wurman, J., 2005. The 30 May 1998 Spencer, South Dakota, Storm. Part I:
546 The Structural Evolution and Environment of the Tornadoes,” AMS Monthly Weather
547 Review, v. 133, 72-96.
- 548 [2]. Baker, C. J., 2007. The debris flight equations. Journal of Wind Engineering and Industrial
549 Aerodynamics 95(5):329-353.
- 550 [3]. Baker, C.J., Sterling, M., 2017. Modelling wind fields and debris flight in tornadoes, J. Wind
551 Eng. and Ind. Aerody., 168, 312-321.
- 552 [4]. Bourriez, F., Sterling, M., Baker, C.J., 2017. Physically modelling windborne debris in tornado-
553 like flow, 9th Asia-Pacific Conference on Wind Engineering, Auckland, New Zealand, 2017.
- 554 [5]. Courant, R., Friedrichs, K., Lewy, H., 1928. Über die partiellen Differenzgleichungen der
555 mathematischen Physik, Mathematische Annalen (in German), 100 (1): 32–74.
- 556 [6]. Darrow, M., 2019. Day 4-8 Severe Weather Outlook Issued on Feb 28, 2019. Norman,
557 Oklahoma: Storm Prediction Center. Retrieved from
558 https://www.spc.noaa.gov/products/exper/day4-8/archive/2019/day4-8_20190228.html
- 559 [7]. English, E. C., Holmes, J. D., 2005. Non-dimensional solutions for trajectories of wind-driven
560 compact objects, Proceedings of The Fourth European and African Conference on Wind
561 Engineering.
- 562 [8]. Evans, S., 2019. U.S. Severe weather in May to drive \$2 Billion or greater financial impact on:
563 AON. Retrieved from [https://www.artemis.bm/news/u-s-severe-weather-in-may-to-drive-
564 2bn-or-greater-financial-impact-aon/](https://www.artemis.bm/news/u-s-severe-weather-in-may-to-drive-2bn-or-greater-financial-impact-aon/)
- 565 [9]. Gairola, A., Bitsuamlak, G., 2019. Numerical tornado modelling for common interpretation of
566 experimental simulators. Journal of Wind Engineering and Industrial Aerodynamics, Volume
567 186, pages 32-48.
- 568 [10]. Gillmeier, S., Hemida, H. and Sterling, M., 2016. An analysis of the influence of a tornado
569 generators geometry on the flow field. 8th International Colloquium on Bluff Body
570 Aerodynamics and Applications June 7 – 11.
- 571 [11]. Gillmeier, S., Sterling, M., Baker, C.J. and Hemida, H., 2017. A reflection on analytical vortex
572 models used to model tornado-like flow fields. International Workshop on Physical Modelling
573 of Flow and Dispersion Phenomena Dynamics of Urban and Coastal Atmosphere.
- 574 [12]. Gillmeier, S., Sterling, M., and Hemida, H (2019). Simulating Tornado-Like Flows – the Effect
575 of the Simulator’s Geometry. Meccanica. Vol. 54, No. 15, 2385-2398,
576 <https://doi.org/10.1007/s11012-019-01082-4>.
- 577 [13]. Hangan, H. and Kim, J.D., 2006. Numerical simulation of Tornado Vortices. The 4th
578 International Symposium on Computational Wind Engineering, Yokohama.
- 579 [14]. Hangan, H. and Kim, J.D., 2008. Swirl ratio effects on tornado vortices in relation to the Fujita
580 scale. WindStruct.11, 291–302.
- 581 [15]. Harms, Associate Writer Nicole. (2019, February 17). Why Are Tornadoes So Terrifying?
582 Retrieved from <https://www.thoughtco.com/tornado-safety-overview-3444293>
- 583 [16]. Holmes, J. D., Baker, C. J., Tamura, Y., 2006. Short note Tachikawa number: A proposal, Journal
584 of Wind Engineering and Industrial Aerodynamics 94, 41-47.

- 585 [17].Holmes, J. D., 2004. Trajectories of spheres in strong winds with application to wind-borne
586 debris, *Journal of Wind Engineering and Industrial Aerodynamics* 92, 9-22.
- 587 [18].Holmes, J. D., English, E. C., Letchford, C., 2004. Aerodynamic forces and moments on cubes
588 and flat plates, with applications to wind-borne debris, *Summary Papers of the 5th*
589 *International Colloquium on Bluff Body Aerodynamics and Applications*, 103-106.
- 590 [19].Howells, P.C., Rotunno, R., Smith, R.R., 1988. A comparative study of atmospheric and
591 laboratory analogue numerical tornado-vortex models. *Quarterly Journal of Royal*
592 *Meteorological Society* 114, 801–822
- 593 [20].ICEM, C., 2012. ver. 14.0. ANSYS Inc., Southpointe, 275.
- 594 [21].Ishihara, T. and Liu, Z.Q., 2014. Numerical study on dynamics of a tornado-like vortex with
595 touching down by using the LES turbulence model. *Wind and Structures*, Vol, 19, No. 1 000-
596 000.
- 597 [22].Ishihara, T., Oh, S. and Tokuyama, Y., 2011. Numerical study on flow fields of tornado-like
598 vortices using the LES turbulence model. *Journal of Wind engineering and Industrial*
599 *Aerodynamics* 99, 239–248.
- 600 [23].Kosiba, K. A., Robinson, P., Chan, P. W., & Wurman, J. (2014). Wind Field of a Non mesocyclone
601 Anti cyclonic Tornado Crossing the Hong Kong International Airport. *Advances in Meteorology*,
602 1-7.
- 603 [24].Kuai, L., Haan, F.L., Gallus, W.A. and Sarkar, P.P., 2008. CFD simulations of the flow field of a
604 laboratory-simulated tornado for parameter sensitivity studies and comparison with field
605 measurements. *Wind and Structures*. 11, 1-22.
- 606 [25].Kuai, L., Haan, F.L., Gallus, W.A. and Sarkar, P.P., 2008. CFD simulations of the flow field of a
607 laboratory-simulated tornado for parameter sensitivity studies and comparison with field
608 measurements. *Wind and Structures*. 11, 1-22.
- 609 [26].Lewellen, D.C., Lewellen, W.S., 2007. Near-surface intensification of tornado vortices. *Journal*
610 *of the Atmospheric Sciences* 64, 2176–2194.
- 611 [27].Lewellen, D.C., Lewellen, W.S., Xia, J., 1999. The influence of a local swirl ratio on tornado
612 intensification near the surface. *Journal of the Atmospheric Sciences*57, 527–544.
- 613 [28].Lin, N., Holms J. D., Letchford, C. W., 2007. Trajectory of windborne debris and applications to
614 impact test-ing, *J. Structural Eng. ASCE*, 133(2), 274-282.
- 615 [29].Liu, Z, Ishihara, T., 2015. Numerical study of turbulent flow fields and the similarity of tornado
616 vortices using large eddy simulations. *Journal of Wind engineering and industrial*
617 *aerodynamics*. 145, 42-60.
- 618 [30].Maruyama, T., 2009. A Numerically Generated Tornado-like Vortex by Large Eddy Simulation,
619 *Proceedings of Seventh Asia-Pacific Conference on Wind Engineering*, Taipei Taiwan, 2009.8,
620 pp. 349-352.
- 621 [31].Maruyama, T., 2011. Simulation of flying debris using a numerically generated tornado-like
622 vortex. *J. Wind Eng. Ind. Aerod.* 99, 249–256.
- 623 [32].Maas H-G, Gruen A., Papantomiou D., 1993. Particle tracking velocimetry in three-dimensional
624 flows. Part I. *Exp Fluid*, 15:133–46.
- 625 [33].Malik N.A., Dracos T., Papantomiou D., 1993. Particle tracking velocimetry in three-
626 dimensional flows. Part II. *Exp Fluid*, 15:279–94.
- 627 [34].Matsui, M., Tamura, Y., Yoshida, A., 2008. Wind pressure distribution around cube in tornadic
628 flow and moving effects on tornadic flow, *Proc. 20th National Symposium on Wind*
629 *Engineering*, pp.319-324 (Japanese).
- 630 [35].Matsui, M., Tamura,Y., 2009. Influence of swirl ratio and incident flow conditions on
631 generation of tornado-like vortex. In: *Proceedings of the 5th European and African Conference*
632 *on Wind Engineering*. CD-ROM.

- 633 [36].Mitsuta, Y., Monji,N., 1984. Development of a laboratory simulator for small scale
634 atmospheric vortices. *Nat. Disaster Sci.*6, 43–54.
- 635 [37].Monji, N., 1985. A laboratory investigation of the structure of multiple vortices. *J. Meteorol.*
636 *Soc. Jpn.* 63, 703–712.
- 637 [38].Natarajan, D., 2011. Numerical Simulation of Tornado-like Vortices. (Unpublished doctoral
638 thesis). University of Western Ontario, Canada.
- 639 [39].Nolan, D.S., Farrell, B.F., 1999. The structure and dynamics of tornado-like vortices. *Journal of*
640 *the Atmospheric Sciences* 56, 2908–2936.
- 641 [40].OpenFOAM, 2019. OpenFOAM: User guide version 7. Retrieved from
642 <http://foam.sourceforge.net/docs/Guides-a4/OpenFOAMUserGuide-A4.pdf>
- 643 [41].Phuc, P.V., Nozu, T., Nozawa, K., Kikuchi, H., 2012. A Numerical Study of the Effects of Moving
644 Tornado-Like Vortex on a Cube. The Seventh International Colloquium on Bluff Body
645 Aerodynamics and Applications (BBAA7) Shanghai, China; September 2-6, 2012.
- 646 [42].Putnam, A., 1961. Integrable form of droplet drag coefficient, *ARS Jnl.*, 31, 1467.
- 647 [43].Smagorinsky, J., 1963. General Circulation Experiments with the Primitive Equations. *Monthly*
648 *Weather Review.* 91 (3): 99–164.
- 649 [44].Refan, Maryam & Hangan, Horia. (2018). Near surface experimental exploration of tornado
650 vortices. *Journal of Wind Engineering and Industrial Aerodynamics.* 175C.
- 651 [45].Richards, P.J., Williams, N., Laing, B., McCarty, M., Pond, M., 2008. Numerical calculation of
652 the 3-dimensional motion of wind-borne debris, *J. Wind Eng. and Ind. Aerody.*, 96, 2188-2202.
- 653 [46].Tachikawa, M., 1983. Trajectories of flat plates in uniform flow with application to wind-
654 generated missiles, *Journal of Wind Engineering and Industrial Aerodynamics* 14, 443-453.
- 655 [47].Tang, Z., Feng, C., Wu, L., Zuo, D., James, D.L. (2018) "Characteristics of tornado-like vortices
656 simulated in a large-scale ward-type simulator." *Boundary-Layer Meteorology*, 166, 327-350.
- 657 [48].Tari, P.H., Gurka, R., Hangan,H., 2010. Experimental investigation of tornado-like Vortex
658 dynamics with swirl ratio: the mean and turbulent flow fields. *J.Wind Eng.*
659 *Ind.Aerodyn.*98,936–944.
- 660 [49]. Van Driest, E.R., 1956. Turbulent flow near a wall, *J. Aeronaut. Sci.*, 23, No. 11, 1007-1011.
- 661 [50].Wang, K. and Letchford, C. W., 2003. Flying debris behaviour, 11th International Conference
662 on Wind Engineering, Lubbock, Texas Proceedings 2, 1663-1670.
- 663 [51].Ward, N. B., 1972. The exploration of certain features of tornado dynamics using a laboratory
664 model. *J. Atmos. Sci.*, 29, 1194-1204.
- 665 [52]. Watkins, S., Mousley, P.D., Hooper, J.D., 2002. Measurement of fluctuating flows using multi-
666 hole probes. Proceedings of the 9th International Congress of Sound and Vibration, Orlando,
667 Florida, USA, 8-11 July, International Institute of Acoustics and Vibration (IIAV).
- 668 [53].Wilson, T., Rotunno, R., 1986. Numerical simulation of a laminar end-wall vortex and boundary
669 layer. *Phys. Fluids* 29, 3993–4005.
- 670 [54].Wills, J. A. B., Lee, B. E., and Wyatt, T. A., 2002. A model of wind-borne debris damage, *Journal*
671 *of Wind Engineering and Industrial Aerodynamics* 90, 555-565.
- 672 [55].Yang, Z., 2015 Large-eddy simulation: Pass, Present and the future. *Chinese Journal of*
673 *Aeronautics*, (2015), 28 (1): 11-24.